

A Synthesis of Data from Fundamental Plane and Surface Brightness Fluctuation Surveys

John P. Blakeslee,^{1,2} John R. Lucey,² Brian J. Barris,³ Michael J. Hudson,⁴
and John L. Tonry³

¹*Department of Physics and Astronomy, Johns Hopkins University, Baltimore, MD 21218, U.S.A.; jpb@pha.jhu.edu*

²*Department of Physics, University of Durham, South Road, Durham, DH1 3LE, United Kingdom; John.Lucey@durham.ac.uk*

³*Institute for Astronomy, University of Hawaii, 2680 Woodlawn Drive, Honolulu, HI 96822, U.S.A.; barris,jt@ifa.hawaii.edu*

⁴*Department of Physics, University of Waterloo, ON, N2L 3G1, Canada; mjhudson@uwaterloo.ca*

Submitted — 30 March 2001. Accepted — 5 July 2001.

ABSTRACT

We perform a series of comparisons between distance-independent photometric and spectroscopic properties used in the surface brightness fluctuations (SBF) and fundamental plane (FP) methods of early-type galaxy distance estimation. The data are taken from two recent surveys: the SBF Survey of Galaxy Distances and the Streaming Motions of Abell Clusters (SMAC) FP survey. We derive a relation between $(V-I)_0$ colour and M_{g_2} index using nearly 200 galaxies and discuss implications for Galactic extinction estimates and early-type galaxy stellar populations. We find that the reddenings from Schlegel et al. (1998) for galaxies with $E(B-V) \gtrsim 0.2$ mag appear to be overestimated by 5–10%, but we do not find significant evidence for large-scale dipole errors in the extinction map. In comparison to stellar population models having solar elemental abundance ratios, the galaxies in our sample are generally too blue at a given M_{g_2} ; we ascribe this to the well-known enhancement of the α -elements in luminous early-type galaxies. We confirm a tight relation between stellar velocity dispersion σ and the SBF ‘fluctuation count’ parameter \overline{N} , which is a luminosity-weighted measure of the total number of stars in a galaxy. The correlation between \overline{N} and σ is even tighter than that between M_{g_2} and σ . Finally, we derive FP photometric parameters for 280 galaxies from the SBF survey data set. Comparisons with external sources allow us to estimate the errors on these parameters and derive the correction necessary to bring them onto the SMAC system. The data are used in a companion paper which compares the distances derived from the FP and SBF methods.

Key words: galaxies: distances and redshifts — galaxies: elliptical and lenticular, cD — galaxies: fundamental parameters — galaxies: stellar content

1 INTRODUCTION

However violent or disturbed in youth, mature elliptical galaxies are remarkably well-behaved members of the celestial pageant. Their photometric and structural properties obey well-defined relations over a very large range in mass and luminosity. The correlations of distance-dependent properties with distance-independent ones then allows for the derivation of galaxy distances.

The fundamental plane (FP) (Dressler et al. 1987; Djorgovski & Davis 1987) works as a distance indicator because elliptical galaxies are dynamically hot systems obeying the virial theorem and have fairly similar, mainly old, stellar populations. The distance-dependent quantity is a combination of the galaxy effective radius and surface brightness

(or just the galaxy luminosity for the Faber-Jackson [1976] relation), and the distance-independent one is the stellar velocity dispersion σ . Sometimes a stellar population term, usually the M_{g_2} index, is also incorporated into the FP (e.g., Guzmán & Lucey 1993).

The surface brightness fluctuations (SBF) distance method (Tonry & Schneider 1988) relies solely on the stellar population properties of old stellar systems; this enables Cepheid calibration via SBF measurements in spiral bulges. The distance-dependent quantity for SBF is the luminosity-weighted mean luminosity of the stellar population and the distance-independent one is the $(V-I)$ colour, or possibly some other stellar population indicator.

This paper examines and compares the various photo-

metric and spectroscopic parameters used in the SBF and FP distance methods. We first discuss the data samples used for this study before exploring correlations between the distance-independent parameters which go into the methods. Special attention is given to potential systematic effects that could bias the distance estimates. We then describe our procedure for deriving the distance-dependent FP photometric parameters from SBF survey imaging data and compare the results with external data in order to evaluate their accuracy. We include a data table listing both the FP and SBF parameters; these are used in a companion paper (Blakeslee et al. 2002, hereafter Paper II) which makes detailed comparisons of the distance estimates for individual galaxies from the two methods.

2 DISTANCE-INDEPENDENT COMPARISONS

For this study, we combine data from two recent early-type galaxy distance surveys: the SBF Survey of Galaxy Distances and the Streaming Motions of Abell Clusters (SMAC) project. The SBF survey data and calibration are described in detail by Tonry et al. (1997, 2000, hereafter SBF-I and SBF-II), with further analysis of the data given by Blakeslee et al. (1999, SBF-III). SBF survey data for 300 galaxies within $cz \lesssim 4000 \text{ km s}^{-1}$ are tabulated by Tonry et al. (2001, SBF-IV). The SMAC project is a cluster FP survey which combines new and literature data into a common system. As well as providing standardised parameters for cluster galaxies, the SMAC project derived improved values for many nearby non-cluster galaxies. The new photometric and spectroscopic data are presented by Smith et al. (2000, 2001, hereafter SMAC-I and SMAC-II), and the full SMAC data set is tabulated by Hudson et al. (2001, SMAC-III). A preliminary analysis of the peculiar velocity data was given by Hudson et al. (1999). Here, we match data for galaxies appearing in both surveys and discuss correlations between the various distance-independent galaxy properties.

2.1 The $(V-I)_0$ - Mg_2 - σ Relations

We matched all galaxies with $(V-I)$ colours from the SBF survey (SBF-IV) against the SMAC spectroscopic catalogue of homogenized Mg_2 and σ measurements. The spectroscopic measurements have been normalized to a standard aperture of radius $r_{\text{ap}} = 0.6 h^{-1} \text{ kpc}$ by assuming a fixed radial gradient from Jorgensen et al. (1995) for all the galaxies and using the observed velocities to approximate distances (see SMAC-III). The $(V-I)$ colours, however, are derived from the regions within the galaxies that were used for the SBF analysis. Because the galaxy centres are usually saturated in the SBF observations and the central regions are frequently affected by dust, these colours roughly correspond to the colour near one effective radius $r \approx R_e$ (aperture effects on the $(V-I)_0$ - Mg_2 relation are discussed in §2.4). Galactic extinction values and ratios from Schlegel, Finkbeiner, & Davis (1998, hereafter SFD) were used in deriving the reddening-corrected $(V-I)_0$ colours (see SBF-II). The adopted reddening law gives $E(V-I) = 1.278E(B-V)$.

A total of 209 galaxies were found to have both $(V-I)$ and Mg_2 data. One of these is M32, which has an extraordinarily large estimated aperture correction, while two others

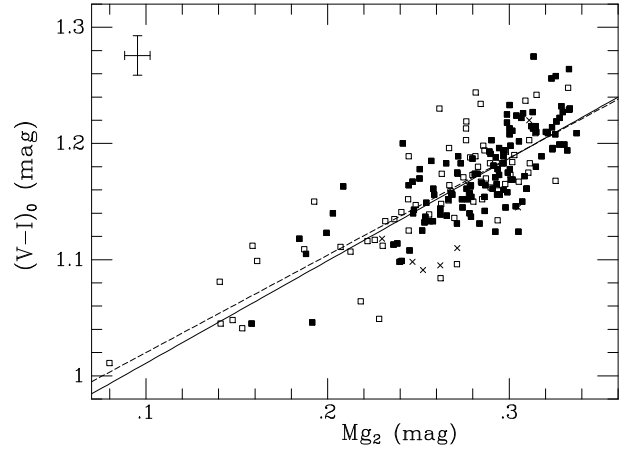


Figure 1. $(V-I)_0$ colour from the SBF survey is plotted against Mg_2 index from the SMAC survey for galaxies in common between the two data sets. Filled squares represent elliptical galaxies (T -type = -5), open squares are S0 galaxies ($T > -5$), and the crosses represent galaxies with relatively high Galactic extinctions ($A_V > 0.5 \text{ mag}$ from SFD). Median measurement errors are shown at upper left. The heavily reddened galaxies are too blue at a given Mg_2 , indicating that their reddenings have been overestimated. The solid and dashed lines are fits to the elliptical and elliptical+S0 samples, respectively.

(NGC 404 and NGC 5102) have $\text{Mg}_2 \lesssim 0.0$. We omit these three galaxies, leaving a sample of 206, all but two (E358-059 and NGC 4468) of which also have SMAC values for σ . The mean observational uncertainties are 0.018 mag in $(V-I)$ (not including reddening errors) and 0.007 mag in Mg_2 ; SBF-I and SMAC-III describe how the errors were estimated from comparisons of repeat observations.

Figure 1 shows the correlation of $(V-I)_0$ with Mg_2 for the cross-matched data set. We find that ellipticals (filled squares, defined as having morphological type $T = -5$ in the RC3 [de Vaucouleurs et al. 1991]), and S0s (open squares, effectively $T > -5$ for this sample) obey the same $(V-I)_0$ - Mg_2 relation. This is expected for a pair of purely stellar population parameters with similar age-metallicity degeneracy properties (e.g., Worthey 1994). However, the 8 highest extinction galaxies (crosses in Figure 1), which have $E(V-I) > 0.20$ and $A_V > 0.52$, preferentially lie below the mean $(V-I)_0$ - Mg_2 relation. The least-squares fits for galaxies with $E(V-I) < 0.20$ and $\text{Mg}_2 > 0.1$ are given by

$$(V-I)_0 = (0.935 \pm 0.014) + (0.843 \pm 0.049) \text{Mg}_2, \quad (1)$$

$$(V-I)_0 = (0.923 \pm 0.019) + (0.881 \pm 0.067) \text{Mg}_2, \quad (2)$$

for all morphological types (197 galaxies, rms scatter 0.0275 mag) and for just the ellipticals (125 galaxies, rms scatter 0.0257 mag), respectively. These fits are clearly identical within the errors.

The 72 S0s exhibit a marginally higher scatter of 0.030 mag , however they also have larger $(V-I)$ measurements uncertainties on average, 0.020 mag compared to 0.017 mag for the ellipticals. Therefore, we assign no physical significance to the marginal difference in scatter. If we perform a bivariate fit using the quoted uncertainties added in quadrature with a cosmic scatter term, we find that the cosmic scatter in $(V-I)_0$ at a fixed Mg_2 must be 0.021 mag to obtain a

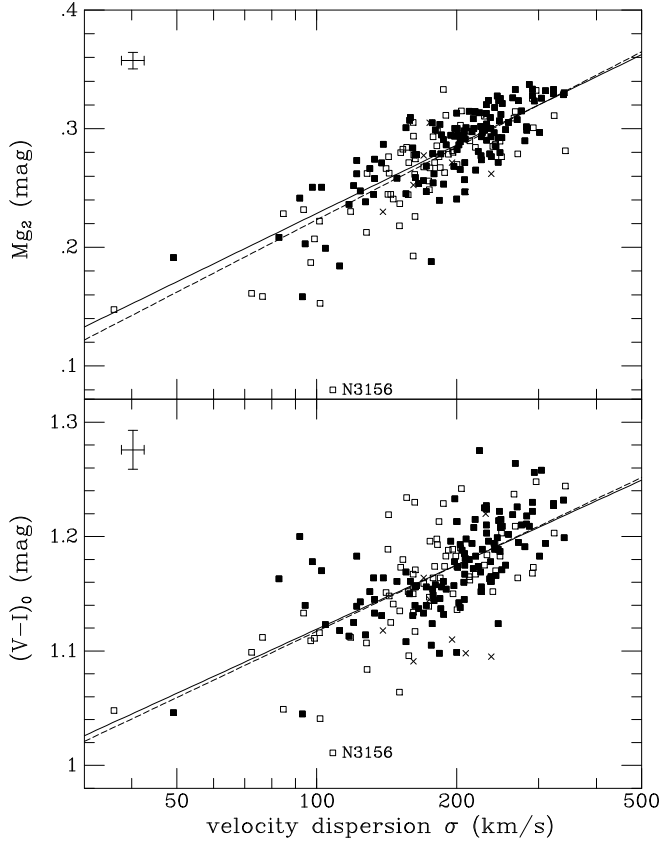


Figure 2. Mg_2 index from the SMAC survey and $(V-I)_0$ colour from the SBF survey are plotted against the central stellar velocity dispersion σ from SMAC. Symbols and lines are as in Figure 1, with median error bars shown at upper left in each panel. The S0 galaxy NGC 3156 with $Mg_2 = 0.08$ is the biggest outlier and has been omitted from the fits. Galaxies with $A_V > 0.5$ mag (crosses) are too blue in $(V-I)_0$ with respect to the average relation, again indicating that their reddenings are overestimated. The $Mg_2 - \sigma$ relation is not sensitive to reddening errors.

reduced χ^2 of unity (or, formally, 0.020 when just the ellipticals are considered and 0.022 for just the S0s). This cosmic scatter actually would include errors resulting from gradient and aperture effects, incorrect reddening estimates, as well as true peculiarities of the stellar populations. In the following section, we use the residuals from the $(V-I)_0$ – Mg_2 relation to investigate problems with the extinction estimates.

Figure 2 plots Mg_2 and $(V-I)_0$ against the stellar velocity dispersion σ for the cross-matched sample. The Mg_2 – σ relation has been discussed in detail by many authors (e.g., Terlevich et al. 1981; Dressler et al. 1987; Guzmán et al. 1992; Bender, Burstein, & Faber 1993; Colless et al. 1999), and we mainly include it here as a comparison to the $(V-I)_0$ – σ relation. Excluding the discordant S0 NGC 3156 which has $Mg_2 < 0.1$, we find

$$Mg_2 = (-0.194 \pm 0.025) + (0.208 \pm 0.011) \log(\sigma), \quad (3)$$

with an rms scatter of 0.022 mag for the full morphological sample (0.021 mag for just the ellipticals), consistent with most previous studies. For the $(V-I)_0$ – σ comparison, we again find that galaxies with $E(V-I) > 0.20$ mag appear to

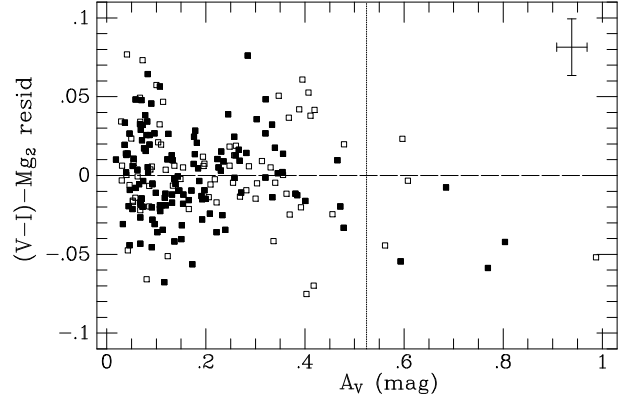


Figure 3. Residuals from a linear fit to the $(V-I)_0$ – Mg_2 relation are plotted against the V -band Galactic extinction value from SFD for ellipticals (filled squares) and S0s (open squares). Median error bars are shown at upper right, where the A_V error estimate is taken from SFD. The vertical dotted line is drawn at $A_V = 0.52$ mag, or $E(V-I) = 0.20$ mag; the eight galaxies at higher extinctions (which were represented by crosses in Figures 1 and 2) tend to lie below the zero-residual line, indicating that their extinctions have been overestimated.

have had their reddening corrections overestimated by SFD. Excluding these and NGC 3156, we find

$$(V-I)_0 = (0.733 \pm 0.033) + (0.192 \pm 0.015) \log(\sigma), \quad (4)$$

with an rms scatter of 0.031 mag for the full morphological sample (again, the elliptical subsample gives a near identical relation and a scatter 0.030 mag). We know of no other published derivations of a $(V-I)$ – $\log \sigma$ relation. However, Bender et al. (1993) presented a relation between $(B-V)_0$ and $\log \sigma$, mainly using the highest quality subsample of 7S data from Burstein et al. (1987). The slope of that relation is also near 0.2 and the scatter is 0.032 mag when the blue galaxies with $(B-V)_0 < 0.8$ are omitted. Bower, Lucey, & Ellis (1992) examined the $(V-K)$ – $\log \sigma$ relation and found scatters of 0.032 and 0.050 mag for samples comprised of 17 Virgo and 31 Coma early-type galaxies, respectively.

2.2 Tests of the Galactic Extinction

We can use the $(V-I)_0$ – Mg_2 relation as a test of the Galactic extinction map. Figure 3 shows the residuals with respect to Eq. (2) and indicates an apparent problem at the highest extinctions: 7 of 8 galaxies (and all 4 ellipticals) with $A_V > 0.5$ have negative residuals. The offset is significant at nearly the 3σ level. In order of increasing extinction, the 8 galaxies are E208-021, NGC 4976, E322-059, E092-013, E221-026, NGC 3136, NGC 2434, and NGC 2380; of these, only E322-059 has a positive residual. There is no simple trend in the residuals at lower extinctions, however. SFD produced a similar plot, showing residuals of the $(B-V)_0$ – Mg_2 relation (data from Faber et al. 1989) against their $E(B-V)$ values. Although they concluded that there was no significant overall trend, all six galaxies with $E(B-V) > 0.2$ had negative residuals. We note that Arce & Goodman (1999) also found that the SFD map overestimates the reddening in regions of smooth extinction with $A_V > 0.5$ mag,

although it may underestimate the reddening in regions with steep extinction gradients.

Hudson (1999) has tested for large-scale systematic errors in extinction maps by fitting dipoles to galaxy $(B-V)_0$ - Mg_2 residuals as a function of position on the sky. He used a sample of 311 galaxies of high photometric quality from Faber et al. (1989) (colours within a radius of $33''$) and the homogenized SMAC Mg_2 values and found weak evidence, at the 92% confidence level, for a dipole residual of 13% amplitude in the SFD extinction map. However, because the residuals with respect to a smaller, independent data set consisting of Galactic globular clusters and RR Lyra stars did not show this dipole, Hudson concluded that the effect actually resulted from a ~ 0.01 mag systematic error in the galaxy colours across the sky.

We have repeated Hudson's analysis, including the Monte Carlo estimations of the significance, using our sample of 205 galaxies with $Mg_2 > 0.1$ mag. Although the sample is smaller, $(V-I)$ is $\sim 28\%$ more sensitive to reddening errors. We do not find a very significant dipole residual. The confidence level for the dipole term in our fit is only 80%, with fractional amplitude 0.09 ± 0.07 . The best-fitting direction, $(l, b) = (97^\circ, -5^\circ)$ in Galactic coordinates, is only 30° from that found by Hudson. However, if just the four highest extinction galaxies, all of which have negative residuals in Figure 3, are omitted, then the fitted dipole swings by more than 60° and has a similar low significance. These four highest extinction galaxies range in l from 241° to 316° and in b from -21.5 to $+12.9$. We conclude that there is no convincing dipole residual in the SFD extinction map from these data, although the extinction values appear to be systematically overestimated in certain directions.

2.3 Environment

We now explore the possibility of environmental influences on the $(V-I)_0$ - Mg_2 relation. Hudson (1999) found that cluster galaxies are 0.01 ± 0.004 mag redder in $(B-V)$ than group/field galaxies at a given Mg_2 . Based on stellar population models, this could imply that cluster ellipticals are older and less enriched at a given Mg_2 , as might be expected in hierarchical formation scenarios. However, such an effect could also imply environmental variations in the abundance ratios, presumably due to differing time-scales for metal enrichment and the relative importance of type I and type II supernovae, with shorter time-scales yielding a higher relative abundance of alpha elements such as Mg (see Worthey 1998 for a discussion). In this case, one would expect cluster ellipticals to have formed more rapidly and thus to have higher Mg_2 at a given $(V-I)_0$, or equivalently, to be bluer at a given Mg_2 .

Figure 4 shows the residuals of the $(V-I)_0$ - Mg_2 relation for galaxies in the field, in the three most prominent clusters, and in other, smaller, groups. The scatter among the Virgo galaxies is the highest, but the sample is weighted more towards lower Mg_2 values than the other samples and may be affected by a couple moderate outliers. Formally, the offset in the $(V-I)_0$ - Mg_2 relation between field and group/cluster galaxies is 0.010 ± 0.005 mag, or 0.012 ± 0.005 mag if Virgo is omitted. This is at the same $\sim 2\sigma$ significance level as found by Hudson (1999), but in the opposite sense: the field galaxies are marginally redder

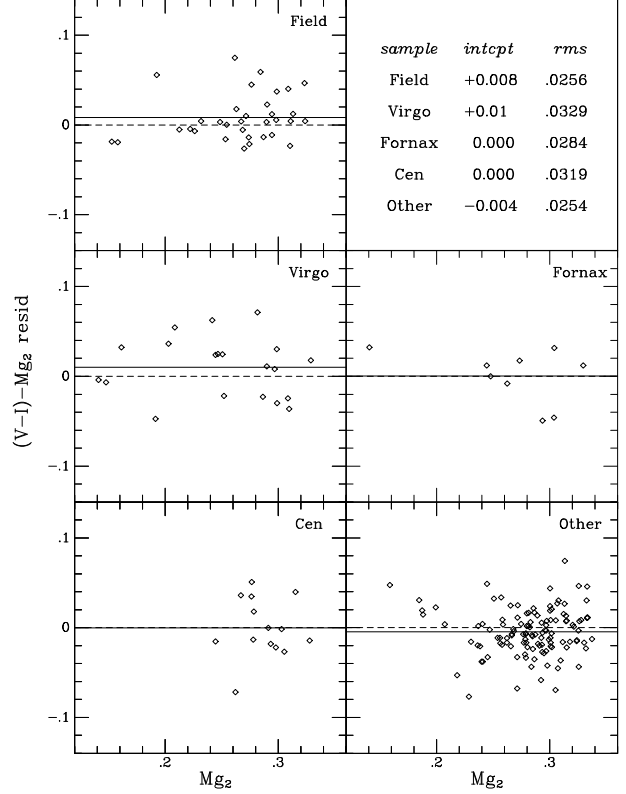


Figure 4. Residuals from a linear fit to the $(V-I)_0$ - Mg_2 relation are plotted against Mg_2 for galaxies in five different environments: the field, Virgo cluster, Fornax cluster, Centaurus (A3526), and other small groups. The vertical intercepts and rms residuals (mag) are listed at upper right.

at a given Mg_2 , which would be consistent with longer enrichment time-scales. However, at this level, systematic directional errors in the extinction will become important, so we do not consider this result significant.

2.4 Comparison to Stellar Population Models

The Mg abundances of giant ellipticals are enhanced with respect to Fe abundances, as compared to the solar ratios (e.g., Worthey, Faber, & Gonzalez 1992). Variations in the Mg to Fe (logarithmic) ratio $[Mg/Fe]$ at a fixed total metallicity and age should cause scatter in the $(V-I)_0$ - Mg_2 relation just as it causes significant scatter in the plots of Fe indices against Mg indices (e.g., Worthey 1998; Kuntschner 2000). The effects of non-solar abundance ratios on broad-band photometric colours due to isochrone temperature and line blanketing effects is not well-modeled, so we decided to look into this in a little more detail.

First it is necessary to make some correction for the systematic difference in aperture between the Mg_2 and $(V-I)_0$ measurements. Most of our galaxies are at distances of 1300 ± 400 km s^{-1} (Virgo, Fornax, Leo, Dorado); at this distance the fiducial radius of $0.6 h^{-1}$ kpc corresponds to $\sim 10''$. We attempted to derive $(V-I)_0$ colours near the galaxy centres using the surface photometry data files described in SBF-I. In many cases this was impossible because of saturation, for instance the images from the CTIO runs

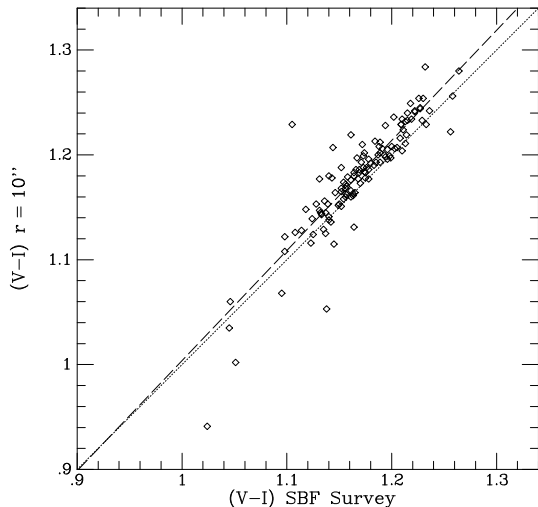


Figure 5. Galaxy colour at a radius $r = 10$ arcsec is plotted against colour from the SBF survey data set for elliptical galaxies. The dotted line is the line of equality, and the dashed line is least-deviation fit to the points. SBF survey colours are typically ~ 0.015 mag bluer than the colour at this fiducial radius.

(see SBF-I) with their large $0''.472$ pixels and severe charge bleeding could not be used for this. For the S0s, the central colours showed large scatter when plotted against the SBF survey colours, owing to dust lanes and irregular gradients associated with disk contamination, etc. However, the relation for the ellipticals was tighter; Figure 5 shows $(V-I)_0$ at $r = 10''$ plotted against $(V-I)_0$ from SBF-IV for the ellipticals (regardless of whether or not they have Mg_2 from SMAC). The least absolute deviation line (to reduce the effect of outliers) shown in the figure is given by

$$(V-I)_0^{\text{ctr}} = 1.05 [(V-I)_0^{\text{SBF}} - 0.92], \quad (5)$$

where ‘ctr’ actually refers to a radius of 10 arcsec. The $(V-I)_0$ aperture correction becomes larger for bigger, redder galaxies, but is always less than 0.02 mag.

However, the Mg_2 value at $r = 10''$ will be ~ 0.01 mag less than the value measured within this radius, according to the mean gradient derived by Jorgensen et al. (1995). Thus, we apply this offset to the Mg_2 indices before making a comparison to the modified colours. In addition, we follow Kuntschner et al. (2001) in ‘correcting’ the Mg_2 indices to what they would be for solar abundance ratios at the same total metallicity Z . We use the results from their sample of 72 early-type galaxies to derive

$$Mg_2^{\text{sol}} = 0.022 + 0.87 Mg_2, \quad (6)$$

where Mg_2^{sol} is the Mg_2 value corrected to solar-abundance ratios. The scatter in this relation is 0.005 mag.

Figure 6 shows the modified $(V-I)_0$ and Mg_2 values as compared to some of the latest (solar abundance ratio) stellar population models from Vazdekis (2001, in preparation; see Blakeslee, Vazdekis, & Ajhar 2001), based on extensive empirical stellar libraries. It is clear that the data do not follow the model locus. In particular, the galaxies with corrected $Mg_2^{\text{sol}} > 0.25$ have colours which are still too blue with respect to the models. The apparent offset in the other direction for $Mg_2^{\text{sol}} < 0.2$ is less worrisome, as this region

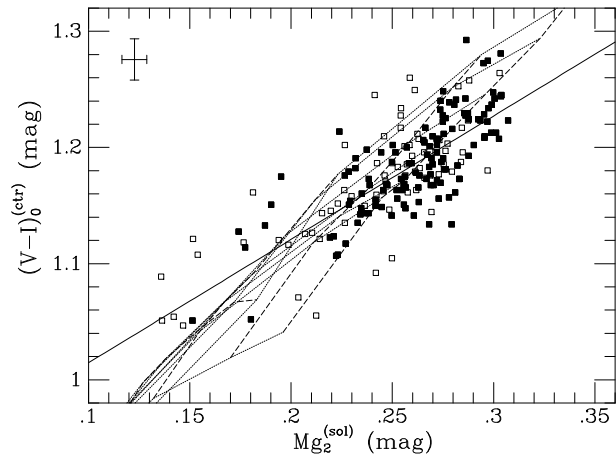


Figure 6. $(V-I)_0$ colour, corrected to the ‘central’ value, is plotted against Mg_2 , corrected to solar abundance ratios following Kuntschner et al. (2001). Filled and open squares are for ellipticals and S0s, respectively. The grid shows updated Vazdekis (1996) stellar population models from Blakeslee, Vazdekis, & Ajhar (2001), with metallicities in the range $[Z/H] = -1.7$ to $+0.2$ dex and ages from 2 to 18 Gyr. The solid line is a fit to the filled points; it has a slope of 1.06, as compared to 0.88 for the corresponding fit in Figure 1. However, the models define a yet steeper slope of ~ 1.5 .

is less well-populated by nice ellipticals with well-defined gradients, and only one of the 72 Kuntschner et al. (2001) galaxies which went into deriving Eq. (6) had $Mg_2 < 0.20$. If the ~ -0.03 mag offset in the colours at high Mg_2^{sol} is due to non-solar abundance ratios, then $(V-I)_0$ colour for early-type galaxies must increase, just as the Fe indices increase (see Trager et al. 2000 and Kuntschner et al. 2001), when corrected to solar ratios (i.e., lower Mg at fixed Z).

There has been much discussion as to whether it is more proper to call Mg and the other alpha elements ‘enhanced’ or the Fe-peak elements ‘depressed’ in giant ellipticals (e.g., Vazdekis et al. 1997; Trager et al. 2000, Kuntschner et al. 2001), but both are relative terms. In any case, our results indicate that $(V-I)_0$ colour is not ‘enhanced’ like Mg in these galaxies, but rather is ‘depressed’ towards the blue, consistent with the results of Salaris & Weiss (1998) who found that isochrones with $[Mg/Fe] > 0$ were hotter, and thus bluer, at all stages in the stellar evolution than scaled-solar abundance isochrones at a given total metallicity. The difference in temperature became much more pronounced for the higher-metallicity isochrones.

2.5 Distance-Independent Mass Measures

SBF-IV introduced the distance-independent ‘fluctuation star count’ \bar{N} , defined as the difference between the SBF magnitude \bar{m} and the total galaxy magnitude:

$$\bar{N} = \bar{m} - m_{\text{tot}} = +2.5 \log \left[\frac{L_{\text{tot}}}{\bar{L}} \right], \quad (7)$$

where L_{tot} is the total luminosity and \bar{L} is the fluctuation luminosity (the luminosity-weighted mean stellar luminosity). Therefore, \bar{N} corresponds to 2.5 times the logarithm of the luminosity-weighted number of stars in a galaxy; as such, it essentially scales with the galaxy mass. Because \bar{m} and

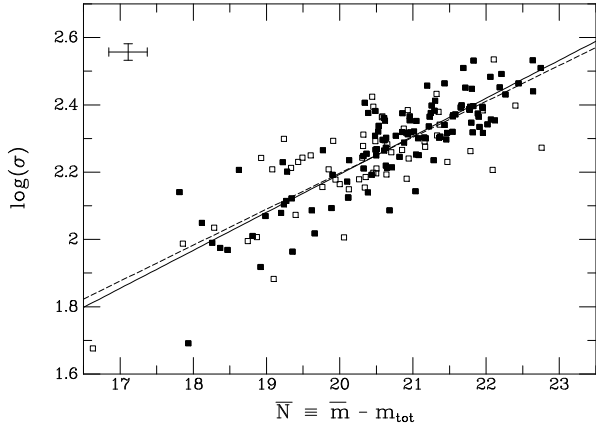


Figure 7. The stellar velocity dispersion σ from the SMAC catalogue is plotted against the ‘fluctuation star count’ parameter \bar{N} discussed by SBF-IV. Filled and open circles are ellipticals and S0s, respectively; the dashed line is a fit to the full sample, and the solid line is a fit the ellipticals.

m_{tot} are measured in the same bandpass, this parameter is independent of Galactic extinction and, if both are from the same image, independent of photometric zero point.

SBF-IV showed that \bar{N} correlated well with the galaxy velocity dispersion for a sample of 64 ellipticals with velocity dispersions from Prugniel & Simien (1996). Figure 7 shows the corresponding plot for 174 SBF survey galaxies with m_{tot} values from the fits described in the following section and SMAC velocity dispersions. The least-squares fit to the ellipticals and S0s with $\bar{N} > 18$ is

$$\log \sigma = 2.20 + 0.10 (\bar{N} - 20), \quad (8)$$

with an rms scatter of 0.079 dex; the 117 ellipticals give a closely consistent result and have a scatter of 0.069 dex. Thus, the relation is even tighter than the $\log \sigma$ – Mg_2 relation, which has a scatter of 0.084 dex for the same sample of galaxies (both the full sample and elliptical subsample).

Eq. (8) is nearly identical to the relation found by SBF-IV for their smaller sample. Rearranging terms, we have

$$L_{\text{tot}} = 10^8 \bar{L} \left(\frac{\sigma}{160 \text{ km s}^{-1}} \right)^{4.0}, \quad (9)$$

which resembles the Faber-Jackson relation, except that the \bar{L} term has a dependence on mass-to-light ratio that results in the small scatter for Eq. (8). Blakeslee et al. (2001) discuss the stellar-population aspects of \bar{N} in more detail. We note that the value of the exponent in Eq. (9) depends on the inverse nature of our least-squares fit. A ‘forward’ fit of \bar{N} as a function of $\log \sigma$ would have given an exponent of about 2.8; ideally, one would do a full maximum-likelihood analysis. The use of \bar{N} for an alternative calibration of the SBF method is discussed in Paper II.

3 FP PHOTOMETRIC PARAMETERS FROM SBF DATA

Relatively few of the SBF survey galaxies with SMAC spectroscopic parameters also have SMAC surface photometry. This is largely because the SMAC project did not use the

surface photometry from the 7S survey (Burstein et al. 1987), which is in the B -band and uncorrected for seeing effects, while it did include the recalibrated and merged 7S spectroscopic data (Davies et al. 1987). Therefore, we have derived FP photometric parameters from SBF survey data. This presented a number of challenges, as the field sizes were not ideal and the galaxy centres often saturated. However, SBF-I described a procedure for measuring surface photometry in a series of concentric circular annuli of $3''$ width for all the SBF survey images after masking and interpolating over the bright stars. The surface photometry data were used in SBF-I to determine accurate photometric offsets for the many individual observing runs in the SBF survey and to provide accurate calibrations for non-photometric survey data.

We fitted Sersic (1968) $r^{1/n}$ profiles to the SBF survey surface photometry data in circular annuli. A generalization of the de Vaucouleurs (1948) law, the $r^{1/n}$ profile is convenient because it describes a large range of galaxy types from exponential disks to highly diffuse cD halos. [See Ciotti & Lanzoni (1997) and Ciotti & Bertin (1999) for discussions of the general properties of stellar systems following $r^{1/n}$ profiles.] This profile has been widely used for empirically characterizing galaxy light distributions (e.g., Davies et al. 1988; Young & Currie 1994; Caon, Capaccioli & D’Onofrio 1993; Courteau et al. 1996), including specifically for measuring FP distances (Graham & Colless 1997; Graham 1998). Kelson et al. (2000) also explored $r^{1/n}$ -law fits and concluded that the difference with respect to the $r^{1/4}$ -law fits was negligible for their subset of SBF survey data; however, the full data set is much more morphologically diverse, so we have kept this extra degree of freedom.

Not all the of the SBF survey galaxies converged to reasonable $r^{1/n}$ fits (reduced $\chi^2 \lesssim 1$). The failures to produce a good fit were partly because of morphological irregularity (9% of the 299 galaxies in the sample presented by SBF-IV were classified as spirals) and partly because of problems in the data (central saturation, bright nearby stars, occasionally poor flattening, etc.) that could be overcome for the SBF analysis, but not for the surface photometry fitting. We fitted the V and I SBF surface photometry down to fixed fractions of the sky brightness, 2.0% in V and 0.4% in I . Acceptable $r^{1/n}$ fits were obtained for a total of 280 galaxies, of which 268 were elliptical or lenticular ($T \leq 0$); 257 of these were successfully fitted in both the V and I bands. The fits were integrated to find the total magnitudes, half light (or effective) radii R_e , and mean surface brightnesses $\langle \mu \rangle_e$ interior to the half light radius.

The surface brightnesses are corrected for Galactic extinction from SFD and $(1+z)^4$ dimming in all cases. We use the same K -corrections as in SBF-I: $1.9z$ for V magnitudes and $1.0z$ for I magnitudes. Because the SMAC survey data are standardised to the R -band, we transform the V and I surface brightnesses to R according to

$$(V-R)_0 = 0.034 + 0.46 (V-I), \quad (10)$$

which comes from the empirically-based models discussed in §2.4. At the median colour of $(V-I)_0 = 1.16$, this implies $(V-R)_0 = 0.57$, identical to the fixed colour transformation used by Smith et al. (1997) and only 0.01 mag different from the fixed color assumed by SMAC-III. As a further check, we derived a rough transformation based on data for 11 early-

type galaxies with VRI colours measured by Tonry, Ajhar, & Luppino (1990), whose $(V-I)_0$ colours span a range of 0.20 mag and share a homogeneous system with our data. The resulting relation has a slope of 0.42 ± 0.06 , consistent with Eq. (10), and is bluer in the mean by 0.015 ± 0.004 mag. This $(V-R)$ zero-point offset is typical of the $(V-I)$ offsets among SBF survey runs prior to homogenization (SBF-II) and is in the opposite sense to the 0.01 mag offset with respect to the SMAC-III colour. We conclude that Eq. (10) is accurate at the 0.01–0.02 mag level.

Finally, we form $X_{\text{FP}} \equiv \log R_e - 0.33\langle\mu\rangle_e$, which is the photometric combination entering into the FP. We have neglected seeing corrections on X_{FP} for this sample of nearby galaxies, all of which have $10'' \lesssim R_e \lesssim 100''$ and were observed in a typical seeing of $1''$.

Table 1 presents the results of our fits to the SBF survey photometry. The columns list: (1) galaxy name and (2) heliocentric velocity as in SBF-IV; (3) morphological T -type from the RC3; (4) B -band extinction from SFD; (5) $(V-I)_0$ colour from the SBF survey; (6) \bar{N} fluctuation count parameter formed from the SBF survey \bar{m}_I and our fitted I -band m_{tot} ; (7) PD quality parameter defined in SBF-II and tabulated in SBF-IV; (8) $\log R_e$ from the I -band fit; (9) mean effective R -band surface brightness $\langle\mu_R\rangle_e$ from the I -band fit; (10) $\log R_e$ from the V -band fit; (11) $\langle\mu_R\rangle_e$ from the V -band fit; (12) $\log \sigma$ from the SMAC survey; and (13) Mg_2 from the SMAC survey. The surface brightnesses are corrected for Galactic extinction and $(1+z)^4$ dimming, K -corrected, and transformed to the R -band as described above. The errors on $(V-I)_0$, $\log \sigma$, and Mg_2 are taken from the SBF and SMAC catalogues. For the \bar{N} error, we added the \bar{m}_I error in quadrature with a nominal 0.2 mag uncertainty in m_{tot} . We have included the PD parameter for further information on the quality of the \bar{m}_I measurement, with high values ($\text{PD} \gtrsim 2.7$) indicating poor quality (see SBF-II and Paper II for discussions). We have not included error estimates on the $\log R_e$ and $\langle\mu\rangle_e$ values, as they are too strongly correlated, and we recommend using them only in the X_{FP} combination. Most of the remainder of this paper is dedicated to evaluating the uncertainty in the X_{FP} values.

Figure 8 shows the comparison between the R -band X_{FP} values determined from the V and I SBF photometry. The overall scatter is 0.023 dex for 257 early-type galaxies. The largest outlier, at 0.014 dex, is NGC 4111, which is a nearly edge-on (axis ratio > 5) S0 galaxy with a red bulge and bluer disk. It does not appear in the 7S or SMAC catalogues and therefore is not used for the distance comparisons in Paper II. Excluding NGC 4111, the scatter in Figure 8 is 0.021 dex. For the 122 ellipticals ($T = -5$), the scatter is 0.016 dex. The internal error per measurements is therefore about 0.015 dex overall, or 0.011 dex for ellipticals. Table 2 summarizes the results of this comparison and the external comparisons below.

4 EXTERNAL FP COMPARISONS

Figures 9 and 10 compare X_{FP} from the I and V SBF surface photometry fits of the previous section to X_{FP} from the SMAC survey. There are 32 galaxies, including 18 ellipticals, with X_{FP} from both data sets. Although our V and I fits were done independently of each other, these figures look

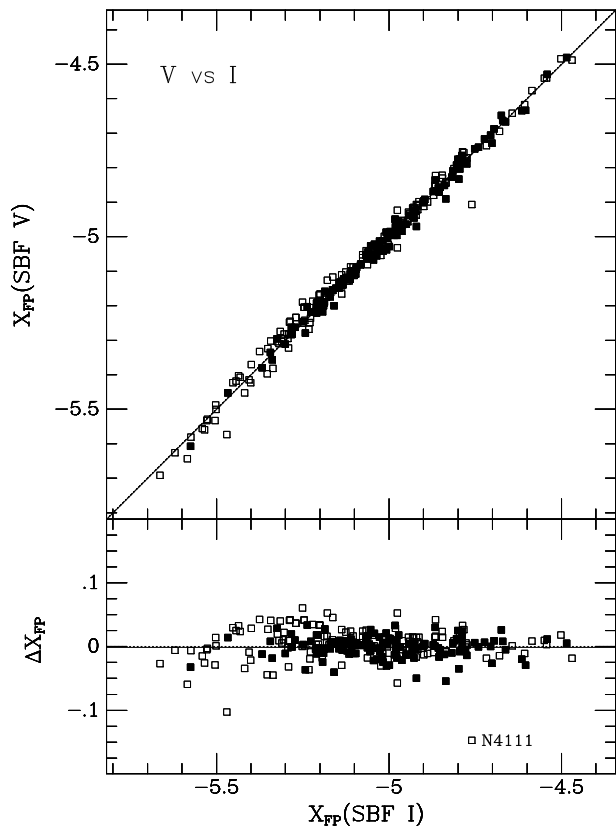


Figure 8. Comparison of the FP photometric parameter $X_{\text{FP}} \equiv \log R_e - 0.33\langle\mu\rangle_e$ determined from V -band and I -band SBF survey surface photometry transformed to the R -band for comparison. The top panel is a direct comparison of X_{FP} for the early-type galaxies, and the lower panel shows the residuals $\Delta = X_{\text{FP}}(\text{SBF } V) - X_{\text{FP}}(\text{SBF } I)$. Open and filled symbols represent S0s and ellipticals, respectively. The dotted lines show equality and the solid lines are fits with unit (top) and zero (bottom) slopes. The overall scatter decreases from 0.023 to 0.021 dex if the edge-on S0 NGC 4111 is omitted; the scatter for just the ellipticals is 0.016 dex.

remarkably similar in detail, not just in their offsets and scatter. This is because the internal scatter is significantly smaller than the external scatter, which has contributions from systematic effects resulting from the different fitting techniques, etc. The biggest outlier in both figures is the Dorado S0 galaxy NGC 1553, which also has the largest X_{FP} in these figures. The data in the SMAC catalogue for this galaxy derive from the Jorgensen et al. (1996) study.

As shown in Table 2, the scatter in X_{FP} for the SMAC–SBF survey comparisons is 0.044 dex for the full overlap sample, 0.039–0.040 dex if NGC 1553 is omitted, and 0.027–0.029 dex for just the ellipticals. The offset between the two sets of X_{FP} values is about 0.030 ± 0.007 dex, in the sense of the SMAC values being larger. In comparison, SMAC-III did not find significant X_{FP} offsets among the different studies which went into the SMAC catalogue. The offset found here is not due to the photometry, as we directly compared photometric zero points for 10 of the 32 galaxies in common (all having new photometry from the SMAC survey), and the systematic offset was 0.03 ± 0.01 mag, a factor of three

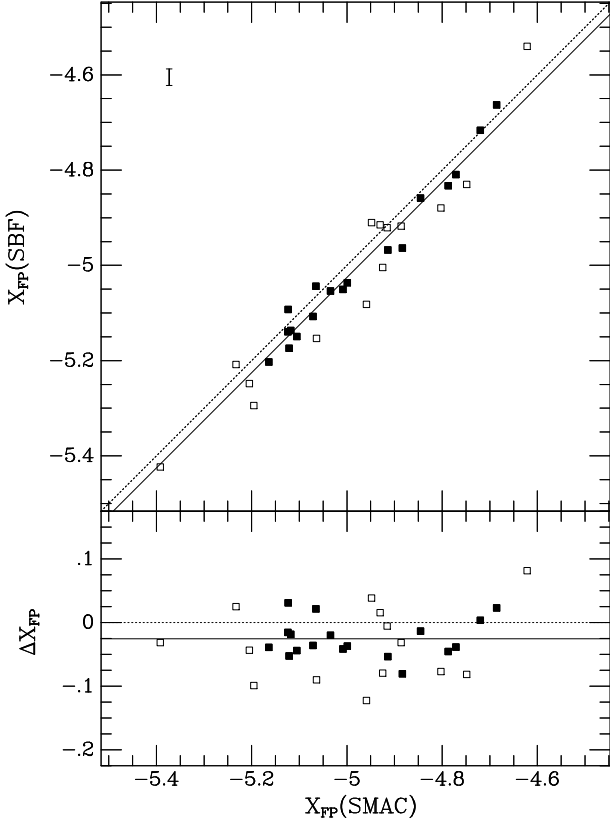


Figure 9. Comparison of the FP photometric parameter $X_{\text{FP}} \equiv \log R_e - 0.33\langle\mu\rangle_e$ determined from the *I*-band SBF survey surface photometry (transformed approximately to the *R* band before calculating X_{FP}) with X_{FP} values determined from the SMAC survey dataset. Top panel is a direct comparison and the lower panel shows the residuals $\Delta = X_{\text{FP}}(\text{SBF}) - X_{\text{FP}}(\text{SMAC})$. Open and filled symbols represent S0s and ellipticals, respectively. The dotted lines show equality and the solid lines are fits with unit (top) and zero (bottom) slopes. A correction of ~ 0.03 dex is required in order to transform the $X_{\text{FP}}(\text{SBF})$ values to the homogeneous SMAC FP system.

too small. Therefore, the X_{FP} offset must come from the difference in fitting procedures used and may partially reflect the lack of seeing corrections. However, the agreement is reasonable after the application of this systematic correction; there is no evidence for systematic trends in the residuals with X_{FP} , redshift, or galaxy type (although the scatter is larger for the S0s).

We can use the 7S photometric data set as an additional external check of our X_{FP} measurements. We downloaded the data from Faber et al. (1989) from the Astronomical Data Center and calculated X_{FP} values from the *B*-band surface brightnesses, $(B-V)$ colours, and effective diameters. The Burstein & Heiles (1984) extinction corrections were removed and the SFD extinction corrections were applied. The surface brightnesses were corrected for $(1+z)^4$ dimming (the 7S catalogue incorrectly states that this was already done), and then transformed to the *R*-band using

$$(V-R)_0 = 0.126 + 0.48(B-V)_0. \quad (11)$$

Since this is an extrapolation of the colours, it is more uncer-

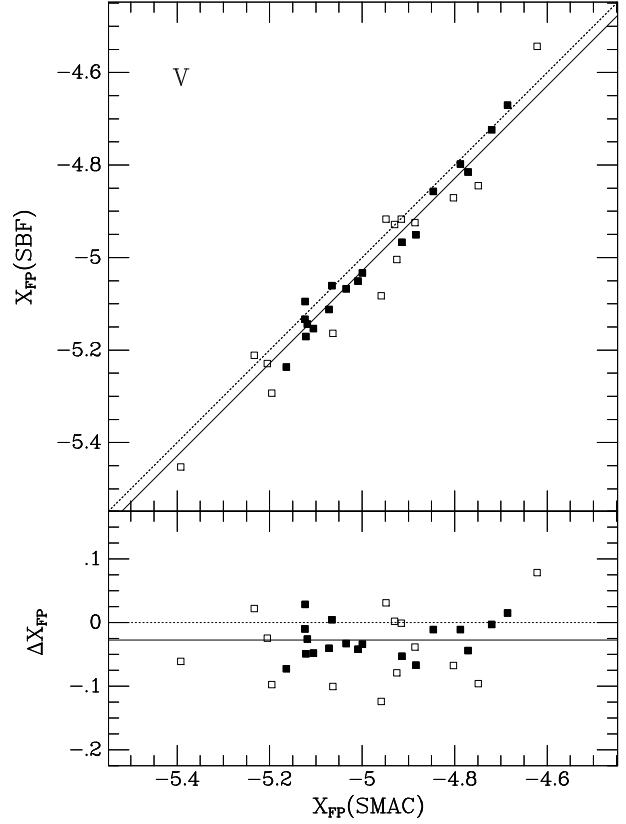


Figure 10. Comparison of the FP photometric parameter $X_{\text{FP}} \equiv \log R_e - 0.33\langle\mu\rangle_e$ determined from the *V*-band SBF survey surface photometry (transformed approximately to the *R* band before calculating X_{FP}) with X_{FP} values determined from the SMAC survey dataset. Top panel is a direct comparison and the lower panel shows the residuals $\Delta = X_{\text{FP}}(\text{SBF}) - X_{\text{FP}}(\text{SMAC})$. Symbols and lines are as in Figure 9. Again, a correction of ~ 0.03 dex is required in order to transform the $X_{\text{FP}}(\text{SBF})$ values to the homogeneous SMAC FP system.

tain than Eq. (10), but the range of galaxy colours is small enough that the typical error in $(B-R)_0$, and hence the *R*-band surface brightness, should only be a few hundredths of a magnitude, or ~ 0.01 dex in X_{FP} .

We noted above that the 7S photometric data were omitted from the SMAC survey because they were not corrected for seeing effects. Figure 11 plots the difference in the X_{FP} values between the SMAC and 7S catalogues against redshift and compares an example SMAC seeing correction curve for a galaxy of fixed physical size $R_e = 1.6 h^{-1}$ kpc ($5''$ at Coma distance) observed in $2''$ seeing. This model appears to overestimate the correction nearby, but gives a good match to the offset at larger distances. Table 2 includes the results of the 7S-SMAC comparison for galaxies within $cz < 5000 \text{ km s}^{-1}$, for which the observed offset is not significant. All of the SBF survey galaxies have $cz < 5000 \text{ km s}^{-1}$ (and only a few have $cz > 4000 \text{ km s}^{-1}$); this is what has allowed us to neglect seeing effects in our own analysis. Before proceeding with the comparisons however, we note that X_{FP} disagreed for NGC 1389 by more than 0.45 dex between the SBF and 7S data sets (it is not in the SMAC photometric catalogue). The $\log R_e$ values agreed to within

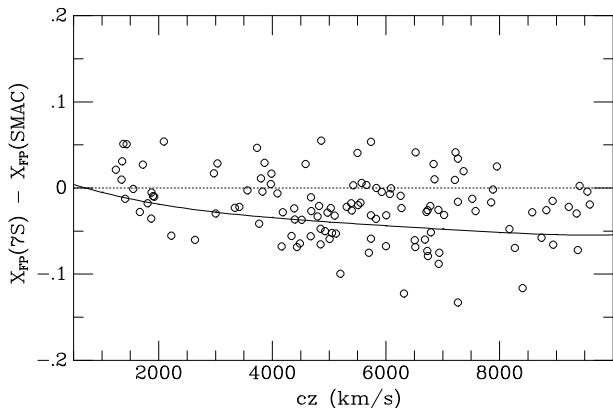


Figure 11. Differences in the X_{FP} parameters between the SMAC and 7S surveys are plotted against heliocentric velocity, used as an indicator of distance. The 7S values have been transformed to the R band with SFD extinction corrections and corrected for $(1+z)^4$ surface brightness dimming. The systematically negative residuals at $cz \gtrsim 5000$ km s $^{-1}$ result from the lack of seeing corrections in the 7S data. The solid curve illustrates example SMAC seeing corrections for a galaxy with $R_e = 1.6$ h $^{-1}$ kpc observed in 2'' seeing at different redshifts.

0.04 dex, but the transformed 7S $\langle\mu\rangle_e$ is fainter by 1.44 mag. This galaxy has ‘quality 3’ (the lowest) photometry in the 7S data set, but other quality 3 galaxies do not show similarly large disagreements, so we omit NGC 1389 only from the comparisons below.

Figures 12 and 13 show the comparisons of the transformed R -band SBF and 7S X_{FP} values. The results are again summarized in Table 2. There is no trend of the residuals with redshift. However, the galaxies which lie significantly below the mean difference line for these SBF-7S comparisons are bluer than average. Figure 14 plots the differences against $(V-I)_0$ colour. Galaxies with $(V-I)_0 \lesssim 1.13$ exhibit greater scatter and tend to have 7S X_{FP} values greater than expected from the comparison to the SBF survey photometry. Table 2 shows that the scatter decreases by $\sim 25\%$ when only $(V-I) \geq 1.135$ galaxies are considered. This could be due to stellar population effects, as the 7S photometry comes from the B -band, while the SBF photometry is in V and I , and both have been transformed to R . However, it is not a simple linear relation between the residuals and colour (there is no trend for the redder galaxies which constitute the bulk of the sample), and photometric transformation errors should not cause offsets in X_{FP} as large as 0.1 dex. We cannot test for a similar problem in the SMAC comparison because the overlapping galaxies all have $(V-I)_0 > 1.13$ (lower panel of Figure 14). We use the X_{FP} values from the SBF survey data and test for colour-dependent errors in the distance analyses of Paper II.

For the purpose of comparison to other works, the last column of Table 2 lists the rms scatters in comparisons of X_{FP} defined with a $\langle\mu\rangle_e$ coefficient of 0.30 instead of 0.33. For instance, Smith et al. (1997) used a coefficient of 0.30 in doing these sorts of X_{FP} comparisons, although the actual calculation of FP distances used a coefficient of 0.326 (Hudson et al. 1997). As Table 2 shows, the magnitude of the scatter is reduced by 20–35% for X_{FP} comparisons us-

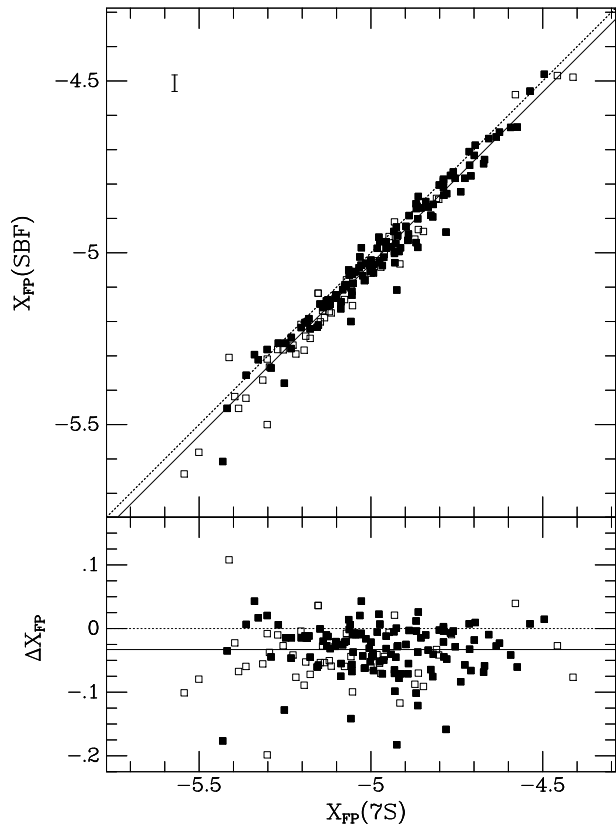


Figure 12. Same as Figure 9 but for the comparison between X_{FP} determined from I -band SBF survey data and X_{FP} determined from the 7S survey dataset of Faber et al. (1989) (both transformed to R band).

ing the smaller coefficient (the scatter would increase by a similar amount if a coefficient of 0.36 were used). The systematic offset of our X_{FP} values would change from ~ 0.030 to ~ 0.020 dex for a $\langle\mu\rangle_e$ coefficient of 0.30 (and to ~ 0.040 dex for a coefficient of 0.36). We have adopted 0.33 for the $\langle\mu\rangle_e$ coefficient in the FP relation because it is within 0.01 of the values derived from very large data samples by Hudson et al. (1997), Jorgensen et al. (1996), Colless et al. (2001) and the SMAC project.

From the various comparisons, we can formally derive the error on X_{FP} for any of the data sets. Specifically, we find that the external errors on our measurements of X_{FP} from SBF survey data are 0.030–0.035 dex, or 0.020–0.025 dex if just the ellipticals are considered, with the 7S X_{FP} errors being about 0.030 dex for both ellipticals and S0s. The X_{FP} errors translate to an error of 6–7% in distance, roughly a factor of 3 smaller than the error expected from the intrinsic scatter in the FP. Thus, our X_{FP} measurements are accurate enough for measuring FP distances, and the systematic correction of 0.03 dex brings them onto the homogeneous SMAC system.

5 SUMMARY

We have merged the SBF survey data with the SMAC FP survey data and explored the correlations between the

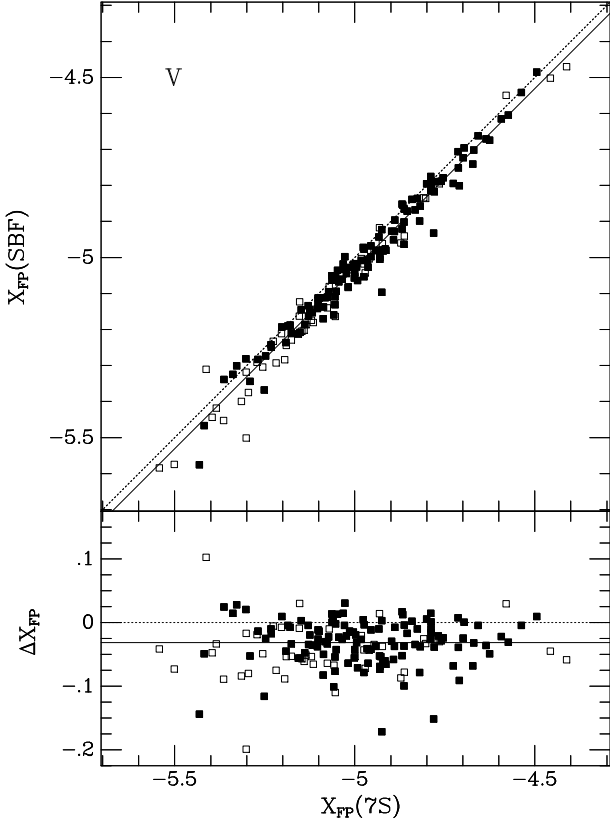


Figure 13. Same as Figure 10 but for the comparison between X_{FP} determined from V -band SBF survey data and X_{FP} determined from the 7S survey dataset of Faber et al. (1989) (both transformed to R band).

distance-independent galaxy properties measured in the two surveys. Using 200 galaxies with data in both catalogues, we derived mean relations between SBF survey $(V-I)_0$ colour and SMAC Mg_2 and velocity dispersions. The intrinsic scatter in the $(V-I)_0$ - Mg_2 relation (including the effects of colour gradients and any reddening errors) is 0.020 mag for the ellipticals and 0.022 mag for the S0s. We used this relation to test for errors in the SFD reddenings. There is no convincing evidence from these data for a dipole residual in the SFD map (our best dipole fit has a 9% amplitude but only 80% confidence). However, we do find that the galaxies in our sample with SFD $A_V \gtrsim 0.55$ mag have overestimated extinctions. Because these galaxies lie near the Galactic plane in a fairly restricted longitude range, we cannot say whether or not the problem is systematic at high extinction or simply indicative of large-scale coherent errors.

We also tested for the influences of environment and α -element enhancement on the $(V-I)_0$ - Mg_2 relation. Consistent with expectations from the α -enhanced isochrone calculations of Salaris & Weiss (1998), we found that the enhancement of the Mg_2 values is not mirrored by redder $(V-I)_0$ colours. In fact, comparison to solar-abundance ratio stellar population models indicates that $(V-I)_0$ is slightly ‘depressed’ at a given total metallicity, and therefore appears to follow the Fe-peak abundances more than the α -elements abundances. We find no evidence for environmental effects larger than 0.01 ± 0.005 mag on the $(V-I)_0$ - Mg_2 relation.

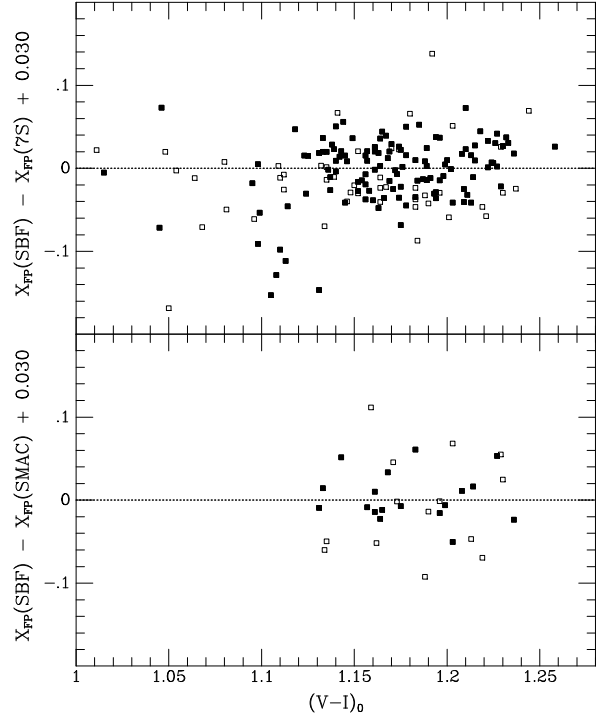


Figure 14. Differences in the X_{FP} values between the 7S and I SBF data sets (top) and between the SMAC and I SBF data sets (bottom) are plotted against $(V-I)_0$ from the SBF survey.

We have derived the relation between the stellar velocity dispersion σ from the SMAC catalogue and the ‘fluctuation star count’ \overline{N} , which was introduced in SBF-IV and corresponds to the luminosity-weighted number of stars in a stellar population. The scatter is only 0.079 dex in $\log \sigma$ (0.069 dex for the ellipticals), making this even tighter than the Mg_2 - $\log \sigma$ relation. The \overline{N} - $\log \sigma$ relation is equivalent to the Faber-Jackson relation with a stellar-population correction term.

Finally, we have used the SBF survey V - and I -band photometry to derive the FP photometric parameters X_{FP} for the survey galaxies. Comparisons to the SMAC and 7S data samples allowed us to estimate the external errors on our X_{FP} measurements. A systematic correction of about 0.03 dex is required to bring our X_{FP} values onto the SMAC photometric system. We provide a full data table of our results, to be used in a forthcoming analysis paper comparing SBF and FP distances to these galaxies.

ACKNOWLEDGMENTS

We thank our SBF and SMAC survey collaborators Ed Ajhar, Roger Davies, Alan Dressler, David Schlegel, and Russell Smith for their help in amassing and processing these data sets. We are grateful to Harald Kuntschner for providing his Mg_2 data in electronic format. This work was supported at the University of Durham by a PPARC rolling grant in Extragalactic Astronomy and Cosmology and made use of Starlink computer facilities. JPB thanks the ACS project at Johns Hopkins University for support while finishing this paper.

REFERENCES

- Arce, H. G. & Goodman, A. A. 1999, *ApJ*, 512, L135
- Bender, R., Burstein, D., & Faber, S. M. 1993, *ApJ*, 411, 153
- Blakeslee, J. P., Davis, M., Tonry, J. L., Dressler, A., & Ajhar, E. A. 1999, *ApJ*, 527, L73 (SBF-III)
- Blakeslee, J. P., Lucey, J. R., Tonry, J. L., Hudson, M. J., Narayanan, V. K., & Barris, B. J. 2002, *MNRAS*, submitted (Paper II)
- Blakeslee, J.P., Vazdekis, A. & Ajhar, E.A. 2001, *MNRAS*, 320, 193
- Bower, R. G., Lucey, J. R., & Ellis, R. S. 1992, *MNRAS*, 254, 601
- Burstein, D., Davies, R. L., Dressler, A., Faber, S. M., Stone, R. P. S., Lynden-Bell, D., Terlevich, R. J. & Wegner, G. 1987, *ApJS*, 64, 601
- Burstein, D. & Heiles, C. 1984, *ApJS*, 54, 33
- Caon, N., Capaccioli, M. & D'Onofrio, M. 1993, *MNRAS*, 265, 1013
- Ciotti, L. & Bertin, G. 1999, *A&A*, 352, 447
- Ciotti, L. & Lanzoni, B. 1997, *A&A*, 321, 724
- Colless, M., Burstein, D., Davies, R. L., McMahan, R. K., Saglia, R. P. & Wegner, G. 1999, *MNRAS*, 303, 813
- Colless, M., Saglia, R. P., Burstein, D., Davies, R. L., McMahan, R. K., & Wegner, G. 2001, *MNRAS*, 321, 277
- Courteau, S., de Jong, R. S. & Broeils, A. H. 1996, *ApJ*, 457, L73
- Davies, J. I., Phillipps, S., Cawson, M. G. M., Disney, M. J. & Kibblewhite, E. J. 1988, *MNRAS*, 232, 239
- Davies, R. L., Burstein, D., Dressler, A., Faber, S. M., Lynden-Bell, D., Terlevich, R. J. & Wegner, G. 1987, *ApJS*, 64, 581
- de Vaucouleurs, G. 1948, *Ann. d'Astroph.*, 11, 247
- de Vaucouleurs, G., de Vaucouleurs, A., Corwin, H. G., Jr., Buta, R. J., Paturel, G., & Fouqué, P. 1991, *Third Reference Catalog of Bright Galaxies* (New York: Springer-Verlag) (RC3)
- Djorgovski, S. & Davis, M. 1987, *ApJ*, 313, 59
- Dressler, A., Lynden-Bell, D., Burstein, D., Davies, R. L., Faber, S. M., Terlevich, R. & Wegner, G. 1987, *ApJ*, 313, 42
- Faber, S. M. & Jackson, R. E. 1976, *ApJ*, 204, 668
- Faber, S. M., Wegner, G., Burstein, D., Davies, R. L., Dressler, A., Lynden-Bell, D. & Terlevich, R. J. 1989, *ApJS*, 69, 763
- Graham, A. W. 1998, *MNRAS*, 295, 933
- Graham, A. & Colless, M. 1997, *MNRAS*, 287, 221
- Guzmán, R. & Lucey, J. R. 1993, *MNRAS*, 263, L47
- Guzmán, R., Lucey, J. R., Carter, D. & Terlevich, R. J. 1992, *MNRAS*, 257, 187
- Hudson, M. J. 1999, *PASP*, 111, 57
- Hudson, M. J., Lucey, J. R., Smith, R. J., Schlegel, D. J., & Davies, R. L. 2001, *MNRAS*, in press (SMAC-III)
- Hudson, M. J., Lucey, J. R., Smith, R. J. & Steel, J. 1997, *MNRAS*, 291, 488
- Hudson, M. J., Smith, R. J., Lucey, J. R., Schlegel, D. J., & Davies, R. L. 1999, *ApJ*, 512, L79
- Jorgensen, I., Franx, M. & Kjaergaard, P. 1995, *MNRAS*, 276, 1341
- Jorgensen, I., Franx, M. & Kjaergaard, P. 1996, *MNRAS*, 280, 167
- Kelson, D. D. et al. 2000, *ApJ*, 529, 768
- Kuntschner, H. 2000, *MNRAS*, 315, 184
- Kuntschner, H., Lucey, J. R., Smith, R. J., Hudson, M. J., & Davies, R. L. 2001, *MNRAS*, 323, 615
- Prugniel, P. & Simien, F. 1996, *A&A*, 309, 749
- Salaris, M. & Weiss, A. 1998, *A&A*, 335, 943
- Schlegel, D. J., Finkbeiner, D. P., & Davis, M. 1998, *ApJ*, 500, 525 (SFD)
- Sersic, J. L. 1968, *Atlas de Galaxias Australes* (Cordoba, Argentina: Observatorio Astronomico)
- Smith, R. J., Lucey, J. R., Steel, J. & Hudson, M. J. 1997, *MNRAS*, 291, 461
- Smith, R. J., Lucey, J. R., Hudson, M. J., Schlegel, D. J., & Davies, R. L. 2000, *MNRAS*, 313, 469 (SMAC-I)
- Smith, R. J., Schlegel, D. J., Lucey, J. R., Hudson, M. J., Baggley, G., & Davies, R. L. 2001, *MNRAS*, in press (SMAC-II)
- Terlevich, R., Davies, R. L., Faber, S. M. & Burstein, D. 1981, *MNRAS*, 196, 381
- Tonry, J. L., Ajhar, E. A., & Luppino, G. A. 1990, *AJ*, 100, 1416
- Tonry, J. L., Blakeslee, J. P., Ajhar, E. A., & Dressler, A. 1997, *ApJ*, 475, 399 (SBF-I)
- Tonry, J. L., Blakeslee, J. P., Ajhar, E. A., & Dressler, A. 2000, *ApJ*, 530, 625 (SBF-II)
- Tonry, J.L., Dressler, A., Blakeslee, J. P., Ajhar, E. A., Fletcher, A., Luppino, G., Metzger, M. R., & Moore, C. 2001, *ApJ*, 546, 681 (SBF-IV)
- Tonry, J. L. & Schneider, D. P. 1988, *AJ*, 96, 807
- Trager, S. C., Faber, S. M., Worthey, G. & Gonzalez, J. J. 2000, 119, 1645
- Vazdekis, A., Casuso, E., Peletier, R. F. & Beckman, J. E. 1996, *ApJS*, 106, 307
- Vazdekis, A., Peletier, R. F., Beckman, J. E. & Casuso, E. 1997, *ApJS*, 111, 203
- Worthey, G. 1994, *ApJS*, 95, 107
- Worthey, G. 1998, *PASP*, 110, 888
- Worthey, G., Faber, S. M. & Gonzalez, J. J. 1992, *ApJ*, 398, 69
- Young, C. K. & Currie, M. J. 1994, *MNRAS*, 268, L11

Table 1. Fundamental Plane Data for SBF Survey Galaxies

Galaxy	v_h	T	A_B	$(V-I)_0 \pm$	$\overline{N} \pm$	PD	$\log R_e^{(I)}$	$\langle \mu_R \rangle_e^{(I)}$	$\log R_e^{(V)}$	$\langle \mu_R \rangle_e^{(V)}$	$\log \sigma \pm$	Mg ₂	\pm
E092-013	1770	-4	0.811	1.164 0.033	19.43 0.23	1.52	1.306	19.621	1.448	20.150	2.230 0.029	0.277	0.008
E183-030	2668	-3	0.376	1.139 0.014	20.94 0.57	3.14	1.375	19.483	1.408	19.491	2.241 0.042	0.256	0.010
E208-021	1003	-3	0.750	1.146 0.018	19.49 0.27	1.43	1.507	19.513	1.457	19.384	2.243 0.047	0.304	0.012
E322-008	3029	-2	0.363	1.205 0.023	20.81 0.54	2.53	1.395	20.086	1.513	20.556
E322-038	3134	-3	0.560	1.242 0.051	20.32 0.32	2.37	1.471	20.765	1.297	20.101	2.311 0.041	0.315	0.014
E322-059	3240	-2	0.796	1.220 0.027	20.57 0.28	3.64	1.600	20.637	1.458	20.188	2.363 0.041	0.311	0.014
E322-088	2606	-2	0.484	1.156 0.034	19.85 0.68	2.46	1.021	18.865	0.963	18.815	2.208 0.041	0.278	0.014
E322-101	2053	0	0.493	1.167 0.023	...	1.99	1.256	20.453	2.207 0.021	0.305	0.008
E323-034	4254	-5	0.535	1.165 0.019	20.86 0.28	2.51	1.335	19.351	1.386	19.504	2.375 0.013	0.293	0.006
E358-006	1358	-4	0.043	1.068 0.020	17.59 0.37	0.97	1.494	21.631	1.041	20.076
E358-059	1030	-3	0.039	1.081 0.016	17.27 0.27	1.02	1.067	20.145	1.008	19.948	...	0.140	0.008
I0745	1135	-2	0.091	0.978 0.010	16.63 0.36	2.33	1.117	20.222	1.205	20.443
I1153	744	-2	0.083	1.197 0.011	18.41 0.28	0.83	1.268	20.276	1.117	19.752
I1459	1624	-5	0.069	1.194 0.018	22.21 0.33	1.49	1.684	19.574	1.718	19.752	2.492 0.042	0.332	0.010
I2006	1340	-5	0.048	1.183 0.018	19.61 0.34	1.45	1.259	19.246	1.274	19.300	2.086 0.013	0.273	0.004
I2311	1836	-5	0.620	1.136 0.027	19.98 0.24	2.09	1.275	18.975	1.238	18.896
I3370	2971	-5	0.404	1.185 0.022	20.91 0.24	2.69	1.425	19.332	1.483	19.560	2.318 0.019	0.257	0.008
I4296	3660	-5	0.266	1.236 0.034	22.64 0.27	3.15	1.683	20.154	1.700	20.203	2.532 0.013	0.330	0.005
I4797	2597	-4	0.340	1.184 0.018	20.59 0.27	1.96	1.331	19.282	1.382	19.266	2.366 0.041	0.302	0.014
I4889	2486	-5	0.228	1.137 0.016	20.64 0.24	1.77	1.356	19.207	1.347	19.173	2.219 0.015	0.254	0.004
I4943	2930	-5	0.221	1.133 0.023	19.23 0.25	2.80	1.153	19.727	1.000	19.209	2.230 0.042	0.256	0.010
I5328	3136	-5	0.062	1.173 0.023	21.16 0.22	2.67	1.411	19.695	1.446	19.818	2.303 0.042	0.294	0.010
N0063	1168	0	0.481	0.979 0.018	18.25 0.37	1.14	1.380	19.974	1.919	21.554
N0185	-227	-5	0.792	1.051 0.017	14.17 0.24	0.01	2.129	20.828
N0221	-200	-6	0.346	1.133 0.007	15.60 0.21	0.01	1.475	17.079	1.453	16.893	1.828 0.009	0.119	0.003
N0274	1729	-3	0.242	1.135 0.020	18.70 0.49	1.68	1.228	19.624	1.519	20.631
N0404	-36	-3	0.253	1.054 0.011	16.63 0.21	0.01	1.711	19.858	1.575	19.424	1.676 0.039	0.016	0.007
N0448	1917	-3	0.261	1.132 0.029	...	1.41	1.163	19.316
N0524	2416	-1	0.357	1.221 0.010	21.56 0.28	1.65	1.551	19.252	1.579	19.365
N0584	1875	-5	0.182	1.157 0.009	20.62 0.28	1.41	1.433	18.915	1.445	18.970	2.295 0.009	0.268	0.003
N0596	1817	-4	0.159	1.135 0.008	20.27 0.22	1.51	1.526	19.789	1.509	19.737	2.179 0.024	0.237	0.006
N0636	1805	-5	0.110	1.156 0.008	20.64 0.24	1.13	1.499	20.067	1.495	20.080	2.212 0.011	0.259	0.006
N0661	3836	-4	0.296	1.164 0.011	19.60 0.31	2.73	1.182	19.340	1.258	19.583	2.250 0.026	0.293	0.008
N0680	2953	-4	0.331	1.189 0.011	20.48 0.45	2.87	1.269	19.306	1.378	19.706	2.292 0.026	0.281	0.008
N0720	1716	-5	0.070	1.214 0.009	21.66 0.25	1.09	1.544	19.402	1.523	19.333	2.392 0.009	0.324	0.004
N0821	1716	-5	0.475	1.196 0.022	20.88 0.24	1.00	1.510	19.627	1.594	19.915	2.288 0.009	0.294	0.004
N0855	600	-5	0.311	1.015 0.018	16.25 0.24	0.23	1.365	20.660	1.246	20.344
N0891	529	3	0.280	1.142 0.017	19.23 0.23	0.36	2.081	21.577	2.110	21.713
N0936	1434	-1	0.152	1.213 0.010	21.78 0.34	0.94	1.838	20.357	1.948	20.663	2.263 0.014	0.276	0.004
N0949	610	3	0.254	0.958 0.011	16.96 0.26	0.44	1.374	20.026	1.611	20.755
N1023	648	-3	0.263	1.193 0.017	20.70 0.24	0.25	1.706	19.161	1.667	19.011	2.259 0.030	0.298	0.009
N1052	1475	-5	0.115	1.213 0.010	20.63 0.33	1.48	1.431	19.090	1.390	18.974	2.302 0.032	0.300	0.007
N1162	2331	-5	0.206	1.173 0.032	20.63 0.34	1.91	1.245	19.585	1.294	19.758
N1172	1669	-4	0.275	1.112 0.032	19.40 0.24	1.40	1.664	21.203	1.991	22.321	2.073 0.039	0.230	0.007
N1199	2705	-5	0.234	1.188 0.012	20.93 0.38	2.03	1.420	19.753	1.400	19.728	2.313 0.039	0.293	0.007
N1201	1720	-2	0.070	1.178 0.009	20.54 0.35	2.04	1.557	19.725	1.503	19.546
N1209	2619	-5	0.163	1.198 0.010	21.01 0.30	1.72	1.253	19.050	1.187	18.829	2.321 0.055	0.301	0.010
N1297	1550	-2	0.119	1.187 0.018	20.25 0.46	1.42	1.578	20.915	1.853	21.832
N1316	1780	-2	0.090	1.132 0.016	22.65 0.25	1.79	1.964	19.541	1.986	19.663
N1332	1469	-3	0.137	1.222 0.010	21.37 0.26	1.01	1.450	18.851	1.477	18.950
N1336	1466	-3	0.049	1.124 0.032	18.46 0.25	1.45	1.606	21.632	1.533	21.395
N1339	1380	-4	0.057	1.134 0.012	19.07 0.40	0.95	1.189	19.220	1.278	19.523	2.208 0.012	0.294	0.003
N1344	1217	-5	0.078	1.135 0.011	20.52 0.35	0.97	1.521	19.308	1.474	19.130
N1351	1539	-3	0.061	1.148 0.016	19.76 0.24	1.12	1.539	20.343	1.589	20.516	2.156 0.014	0.262	0.004
N1366	1310	-2	0.073	1.095 0.018	18.93 0.34	1.48	1.230	19.383	1.316	19.745
N1373	1385	-4	0.061	1.085 0.013	17.48 0.50	2.05	1.004	19.797	1.028	19.863
N1374	1397	-5	0.061	1.146 0.016	19.77 0.22	1.00	1.375	19.384	1.404	19.533	2.265 0.014	0.304	0.004
N1375	773	-2	0.062	1.070 0.019	17.93 0.22	0.51	1.174	19.943	1.156	19.960
N1379	1408	-5	0.052	1.143 0.019	19.89 0.23	1.00	1.465	19.722	1.476	19.807	2.094 0.015	0.248	0.004
N1381	1751	-2	0.059	1.189 0.018	19.44 0.28	1.16	1.200	18.842	1.238	18.960
N1382	1763	-3	0.074	1.106 0.013	17.80 0.36	2.58	1.182	20.471	1.196	20.202
N1387	1302	-3	0.056	1.208 0.047	20.79 0.24	1.16	1.551	19.618	1.747	20.372
N1389	950	-3	0.045	1.145 0.019	19.60 0.26	0.91	1.166	18.718
N1395	1702	-5	0.100	1.215 0.010	21.83 0.24	1.49	1.690	19.676	1.647	19.520	2.396 0.014	0.312	0.003

Table 1. Fundamental Plane Data for SBF Survey Galaxies — *continued*

Galaxy	v_h	T	A_B	$(V-I)_0$	\pm	\overline{N}	\pm	PD	$\log R_e^{(I)}$	$\langle\mu_R\rangle_e^{(I)}$	$\log R_e^{(V)}$	$\langle\mu_R\rangle_e^{(V)}$	$\log \sigma$	\pm	Mg ₂	\pm
N1399	1422	-5	0.056	1.227	0.016	21.69	0.24	1.34	1.581	18.920	1.619	19.061	2.509	0.013	0.329	0.003
N1400	549	-3	0.279	1.170	0.009	20.93	0.38	0.32	1.470	19.461	1.500	19.641	2.385	0.018	0.287	0.004
N1404	1925	-5	0.049	1.224	0.016	21.54	0.26	2.00	1.440	18.449	1.480	18.650	2.366	0.012	0.304	0.003
N1407	1766	-5	0.298	1.222	0.010	22.44	0.32	1.42	1.761	19.837	1.722	19.725	2.464	0.019	0.328	0.005
N1419	1557	-5	0.056	1.110	0.018	17.81	0.30	1.63	1.056	19.503	0.988	19.260	2.141	0.029	0.242	0.006
N1426	1443	-5	0.072	1.161	0.009	20.10	0.26	1.27	1.485	20.104	1.476	20.090	2.172	0.025	0.258	0.006
N1427	1430	-4	0.051	1.152	0.018	20.50	0.30	1.45	1.598	20.174	1.549	20.006	2.197	0.018	0.244	0.005
N1439	1670	-5	0.129	1.131	0.009	20.38	0.24	1.25	1.674	20.840	1.893	21.605	2.140	0.022	0.271	0.005
N1521	4165	-5	0.176	1.152	0.029	22.12	0.41	2.81	1.515	20.378	1.523	20.397	2.354	0.029	0.274	0.006
N1527	1165	-3	0.054	1.230	0.016	20.50	0.28	0.95	1.474	19.378	1.493	19.424	2.211	0.025	0.262	0.007
N1537	1371	-3	0.107	1.096	0.018	20.45	0.26	1.72	1.547	19.652	2.198	0.029	0.271	0.006
N1543	1088	-2	0.117	1.173	0.016	20.92	0.24	1.11	1.711	20.086	1.685	20.029	2.181	0.025	0.280	0.007
N1549	1153	-5	0.055	1.168	0.016	21.54	0.25	1.13	1.752	19.601	1.815	19.814	2.320	0.019
N1553	1280	-2	0.053	1.159	0.016	21.47	0.24	1.31	1.533	18.403	1.555	18.480	2.230	0.036	0.268	0.010
N1574	1042	-3	0.070	1.162	0.016	20.87	0.28	1.10	1.590	19.455	1.717	19.884	2.329	0.036	0.290	0.010
N1587	3667	-5	0.308	1.215	0.012	21.43	0.87	3.33	1.339	19.578	1.323	19.502	2.341	0.039	0.315	0.007
N1596	1523	-2	0.041	1.171	0.016	19.33	0.24	1.57	1.211	18.563	1.209	18.599	2.212	0.036	0.275	0.010
N1653	4343	-4	0.178	1.167	0.011	21.37	0.32	3.00	1.407	20.151	1.408	20.157	2.342	0.055	0.284	0.010
N1700	3881	-5	0.185	1.163	0.011	21.57	0.24	2.88	1.344	19.213	1.301	19.027	2.372	0.009	0.279	0.004
N2271	2588	-3	0.527	1.234	0.029	20.64	0.32	1.93	1.241	19.300	1.246	19.296	2.194	0.047	0.284	0.012
N2293	1994	-1	0.518	1.237	0.013	20.44	0.45	2.03	1.664	20.284	1.488	19.714	2.424	0.020	0.309	0.005
N2305	3571	-5	0.327	1.225	0.027	20.61	0.27	3.60	1.561	20.254	1.473	19.958	2.361	0.047	0.299	0.012
N2325	2248	-5	0.508	1.164	0.014	21.03	0.24	2.14	1.747	20.609	1.568	20.059	2.143	0.036	0.287	0.008
N2380	1775	-2	1.318	1.110	0.009	21.17	0.40	1.63	1.613	19.567	1.537	19.313	2.291	0.029	0.271	0.008
N2434	1327	-5	1.073	1.098	0.055	20.53	0.25	1.43	1.633	19.868	1.565	19.674	2.321	0.022	0.247	0.008
N2549	1056	-2	0.282	1.163	0.012	18.85	0.34	1.39	1.229	18.687	1.238	18.663
N2592	1989	-5	0.261	1.205	0.010	19.37	0.47	2.26	1.028	18.893	1.122	19.147
N2634	2269	-5	0.094	1.154	0.022	20.50	0.70	2.22	1.636	21.126	1.605	21.056	2.250	0.017	0.279	0.004
N2681	715	0	0.098	1.041	0.010	20.27	0.39	0.74	1.949	20.926	1.892	20.718
N2695	1825	-2	0.077	1.183	0.051	20.32	0.38	1.64	1.279	19.599	1.312	19.692	2.278	0.055	0.311	0.010
N2699	1825	-5	0.087	1.152	0.051	19.27	0.24	1.68	1.030	18.855	0.962	18.705	2.114	0.055	0.266	0.010
N2768	1363	-5	0.192	1.144	0.027	21.04	0.28	0.96	1.604	19.515	1.589	19.561	2.252	0.021	0.262	0.005
N2784	708	-2	0.927	1.188	0.023	20.29	0.30	1.37	1.608	18.743	1.671	18.961
N2787	689	-1	0.567	1.194	0.019	18.75	0.40	1.18	1.392	18.622	1.520	19.111
N2865	2581	-5	0.356	1.105	0.019	20.82	0.26	2.14	1.439	19.838	1.488	19.954	2.246	0.008	0.188	0.003
N2904	2387	-3	0.544	1.201	0.041	19.28	0.24	2.07	1.203	19.658	1.146	19.483
N2950	1327	-2	0.072	1.110	0.019	19.32	0.32	2.23	1.360	18.968	1.378	18.988
N2962	2117	-1	0.249	1.176	0.017	20.32	0.38	2.06	1.569	20.647	1.700	21.174
N2974	1924	-5	0.235	1.203	0.015	20.96	0.30	2.15	1.656	20.060	1.575	19.774	2.366	0.023	0.290	0.004
N3031	-38	2	0.347	1.187	0.011	19.07	0.32	0.04	1.405	16.930	1.412	17.041
N3032	1561	-2	0.073	1.073	0.019	18.78	0.33	1.71	1.525	20.979	1.311	20.195
N3056	1047	-1	0.386	1.073	0.023	17.90	0.30	1.98	1.310	19.510	1.613	20.391
N3073	1154	-3	0.044	1.007	0.019	18.29	0.94	1.51	1.417	21.538	1.362	21.291
N3078	2506	-5	0.307	1.209	0.017	21.66	0.35	2.67	1.522	19.769	1.563	19.900	2.399	0.019	0.321	0.005
N3087	2662	-4	0.454	1.164	0.019	21.32	0.27	2.23	1.501	19.770	1.360	19.281	2.433	0.055	0.279	0.010
N3115	698	-3	0.205	1.183	0.010	20.46	0.21	0.95	1.590	18.418	1.595	18.379	2.394	0.009	0.289	0.003
N3136	1647	-5	1.027	1.095	0.033	21.24	0.25	1.39	1.722	19.848	1.700	19.751	2.376	0.022	0.262	0.008
N3156	1296	-2	0.148	1.011	0.011	18.28	0.24	1.34	1.274	19.950	1.193	19.732	2.035	0.039	0.080	0.007
N3193	1378	-5	0.111	1.174	0.009	21.36	0.26	0.85	1.472	19.603	1.453	19.506	2.302	0.055	0.282	0.010
N3226	1275	-5	0.098	1.178	0.015	20.59	0.30	1.33	1.792	21.199	2.296	0.039	0.294	0.007
N3245	1358	-2	0.108	1.139	0.023	20.03	0.26	1.79	1.302	18.844	1.381	19.129
N3250	2883	-5	0.445	1.226	0.019	22.26	0.24	2.14	1.451	19.322	1.418	19.212	2.431	0.018	0.308	0.006
N3257	3023	-3	0.334	1.192	0.041	19.77	0.27	2.61	1.100	19.409	1.060	19.304
N3258	2808	-5	0.362	1.209	0.034	21.20	0.30	2.32	1.603	20.439	1.565	20.309	2.457	0.017	0.337	0.005
N3268	2761	-5	0.446	1.189	0.023	21.29	0.30	1.85	1.638	20.585	1.608	20.517	2.383	0.033	0.318	0.009
N3309	4068	-5	0.344	1.208	0.021	21.79	0.70	3.40	1.335	19.613	1.375	19.754	2.395	0.013	0.325	0.005
N3311	3713	-4	0.343	1.229	0.034	22.76	0.53	3.12	2.098	22.138	2.003	21.861	2.272	0.021	0.333	0.010
N3368	899	2	0.109	1.145	0.015	20.23	0.28	1.63	1.698	19.140	1.713	19.241
N3377	689	-5	0.148	1.114	0.009	19.24	0.21	0.89	1.610	19.715	1.618	19.748	2.105	0.006	0.238	0.002
N3379	922	-5	0.105	1.193	0.015	20.48	0.21	1.59	1.708	19.217	1.657	18.973	2.308	0.005	0.289	0.002
N3384	728	-3	0.114	1.151	0.018	20.13	0.22	1.24	1.755	19.802	1.645	19.467	2.149	0.009	0.266	0.003
N3412	867	-2	0.121	1.111	0.015	18.74	0.23	1.40	1.375	19.035	1.700	20.063	1.995	0.011	0.207	0.004
N3414	1476	-2	0.104	1.149	0.019	20.63	0.38	1.66	1.546	19.927	1.619	20.200
N3457	1156	0	0.135	1.098	0.015	1.32	1.036	18.861

Table 1. Fundamental Plane Data for SBF Survey Galaxies — *continued*

Galaxy	v_h	T	A_B	$(V-I)_0$	\pm	\overline{N}	\pm	PD	$\log R_e^{(I)}$	$\langle\mu_R\rangle_e^{(I)}$	$\log R_e^{(V)}$	$\langle\mu_R\rangle_e^{(V)}$	$\log \sigma$	\pm	Mg ₂	\pm
N3489	693	−1	0.071	1.041	0.023	18.87	0.22	0.96	1.287	18.252	1.296	18.222	2.007	0.010	0.153	0.004
N3585	1491	−5	0.278	1.160	0.016	21.46	0.26	2.31	1.755	19.685	1.741	19.640	2.317	0.026	0.297	0.007
N3599	850	−2	0.089	1.112	0.012	19.10	0.26	1.14	1.620	21.183	1.720	21.574	1.883	0.039	0.159	0.007
N3605	686	−5	0.089	1.118	0.024	18.12	0.34	1.11	0.997	19.116	0.987	19.052	2.049	0.039	0.184	0.007
N3607	951	−2	0.090	1.152	0.010	21.35	0.25	1.40	1.620	19.378	1.607	19.400	2.379	0.039	0.285	0.007
N3608	1197	−5	0.090	1.156	0.009	20.51	0.23	0.92	1.546	19.875	1.604	20.094	2.269	0.009	0.295	0.004
N3610	1765	−5	0.043	1.108	0.015	19.91	0.28	2.21	1.329	18.997	1.302	18.893	2.192	0.032	0.245	0.006
N3613	2054	−5	0.053	1.175	0.015	20.97	0.44	2.22	1.502	19.788	1.363	19.279	2.319	0.039	0.271	0.007
N3617	2224	−4	0.213	1.050	0.023	19.15	0.32	3.07	1.465	21.106	1.464	21.107
N3640	1302	−5	0.191	1.140	0.009	21.28	0.23	1.49	1.579	19.531	1.553	19.455	2.236	0.039	0.247	0.007
N3641	1758	−5	0.182	1.131	0.012	18.62	0.31	1.90	1.407	21.258	1.240	20.653	2.207	0.055	0.284	0.010
N3818	1498	−5	0.155	1.124	0.015	20.32	0.63	1.69	1.346	19.886	1.434	20.142	2.248	0.010	0.305	0.005
N3904	1750	−5	0.311	1.156	0.055	20.96	0.24	1.51	1.374	19.014	1.381	19.037	2.354	0.021	0.293	0.006
N3923	1607	−5	0.358	1.194	0.055	21.91	0.23	1.50	1.690	19.382	1.706	19.429	2.334	0.021	0.297	0.006
N3928	974	3	0.085	1.096	0.015	17.95	0.66	1.47	1.107	19.285	1.211	19.631
N3941	944	−2	0.091	1.125	0.013	19.28	0.26	1.63	1.322	18.464	1.366	18.606
N3962	1822	−5	0.201	1.145	0.023	21.96	0.52	2.85	1.795	20.545	1.683	20.190	2.317	0.039	0.298	0.007
N3990	705	−3	0.069	1.151	0.019	0.98	0.967	18.855
N3998	1028	−2	0.069	1.194	0.011	19.84	0.27	1.35	1.353	18.712	1.458	19.102
N4024	1694	−3	0.182	1.141	0.016	20.00	0.51	3.44	1.185	19.098	1.452	20.043	2.165	0.039	0.241	0.007
N4033	1521	−5	0.205	1.113	0.023	18.98	0.28	2.56	1.266	19.593	1.326	19.652	2.070	0.039	0.236	0.007
N4105	1882	−5	0.263	1.171	0.017	21.25	0.24	1.89	1.627	19.914	1.573	19.699	2.398	0.028	0.292	0.006
N4111	806	−1	0.063	1.096	0.015	19.07	0.30	1.20	1.267	18.709	1.155	17.923
N4125	1340	−5	0.082	1.174	0.011	21.80	0.31	1.86	1.772	19.890	1.875	20.241	2.347	0.055	0.281	0.010
N4138	835	−1	0.060	1.164	0.013	18.95	0.32	1.01	1.272	19.000	1.294	19.114
N4150	244	−2	0.078	1.071	0.017	18.06	0.30	0.81	1.189	19.020	1.290	19.400
N4203	1117	−3	0.052	1.195	0.019	20.73	0.25	1.26	1.945	20.940	1.953	20.950
N4233	2371	−2	0.103	1.191	0.015	20.30	0.95	2.43	1.203	19.364	1.342	19.891
N4261	2200	−5	0.078	1.258	0.014	22.06	0.27	1.28	1.505	19.321	1.380	18.892	2.483	0.010	0.326	0.005
N4278	643	−5	0.123	1.161	0.012	20.39	0.27	0.66	1.477	18.912	1.528	19.141	2.376	0.010	0.276	0.005
N4283	1076	−5	0.109	1.178	0.010	18.26	0.27	1.65	0.992	18.648	1.026	18.775	1.990	0.039	0.251	0.007
N4291	1715	−5	0.158	1.175	0.017	20.35	0.37	1.68	1.294	19.154	1.378	19.489	2.406	0.055	0.299	0.010
N4339	1298	−5	0.110	1.200	0.015	19.35	0.26	2.07	1.439	19.994	1.575	20.488	1.964	0.039	0.242	0.007
N4346	762	−2	0.056	1.158	0.012	19.00	0.25	1.00	1.254	18.918	1.411	19.433
N4365	1240	−5	0.092	1.222	0.017	21.66	0.24	1.35	1.735	19.755	1.771	19.849	2.393	0.009	0.307	0.003
N4373	3392	−3	0.348	1.135	0.023	21.96	0.25	2.81	1.533	19.651	1.557	19.752	2.384	0.019	0.286	0.008
N4374	1033	−5	0.175	1.191	0.008	21.81	0.22	1.30	1.776	19.427	1.721	19.201	2.448	0.006	0.290	0.002
N4379	1071	−3	0.101	1.185	0.017	18.70	0.44	1.42	1.196	19.043	1.209	19.102
N4382	758	−1	0.134	1.150	0.022	22.09	0.22	0.76	2.029	20.216	2.179	20.674	2.207	0.015	0.193	0.006
N4386	1649	−2	0.166	1.196	0.019	20.30	0.52	1.87	1.310	19.455	1.440	19.932
N4387	583	−5	0.143	1.163	0.011	18.92	0.75	1.46	1.069	18.971	1.030	18.842	1.918	0.031	0.208	0.005
N4391	1337	−3	0.078	1.112	0.015	18.27	0.33	1.38	1.076	19.633	1.302	20.416
N4406	−221	−5	0.128	1.167	0.008	21.82	0.23	0.85	1.991	20.235	2.066	20.491	2.318	0.008	0.247	0.003
N4419	−182	1	0.143	1.126	0.026	19.03	0.29	1.15	1.296	18.816	1.293	18.966
N4434	1068	−5	0.096	1.125	0.015	19.20	0.25	0.61	1.075	19.017	1.122	19.128	2.079	0.016	0.252	0.004
N4441	1439	−1	0.086	1.005	0.012	17.23	0.48	1.51	1.206	20.286	1.199	20.306
N4458	662	−5	0.103	1.140	0.011	18.36	0.22	0.66	1.222	19.709	1.313	19.983	1.975	0.016	0.203	0.004
N4460	558	−1	0.082	1.011	0.015	16.80	0.26	0.88	1.393	20.204	1.861	21.744
N4468	895	−3	0.198	1.045	0.015	17.40	0.23	1.35	1.495	21.378	1.288	20.674	0.141	0.010
N4472	997	−5	0.096	1.218	0.011	22.18	0.21	1.08	1.796	19.020	1.846	19.187	2.452	0.006	0.299	0.002
N4473	2236	−5	0.123	1.158	0.012	20.37	0.23	1.62	1.542	19.169	1.569	19.284	2.255	0.009	0.299	0.003
N4476	1955	−3	0.123	1.048	0.017	17.89	0.24	1.40	1.234	19.744	1.210	19.700	1.564	0.039	0.148	0.007
N4478	1370	−5	0.107	1.164	0.019	19.35	0.33	1.49	1.097	18.320	1.254	18.896	2.122	0.007	0.245	0.003
N4486	1292	−4	0.096	1.244	0.012	22.11	0.24	0.74	1.793	19.192	1.779	19.178	2.535	0.009	0.282	0.004
N4489	960	−5	0.121	1.046	0.015	17.93	0.24	1.48	1.230	19.776	1.408	20.401	1.692	0.010	0.191	0.004
N4494	1350	−5	0.093	1.139	0.010	20.69	0.22	0.91	1.638	19.435	1.724	19.738	2.086	0.055	0.262	0.010
N4526	602	−2	0.096	1.188	0.021	21.06	0.26	0.92	1.587	19.033	1.511	18.762
N4546	1037	−3	0.147	1.155	0.013	19.67	0.28	1.20	1.403	18.945	1.403	18.992
N4550	381	−2	0.168	1.078	0.011	18.41	0.27	1.11	1.118	18.659	1.149	18.833
N4551	1198	−5	0.166	1.170	0.009	18.81	0.26	1.05	1.171	19.151	1.150	19.078	2.011	0.016	0.251	0.004
N4552	322	−5	0.177	1.194	0.015	20.49	0.23	1.35	1.437	18.682	1.461	18.674	2.382	0.008	0.297	0.003
N4564	1165	−5	0.151	1.161	0.009	19.28	0.26	1.12	1.264	18.796	1.337	19.030	2.201	0.009	0.310	0.003
N4565	1227	3	0.067	1.128	0.027	21.04	0.23	0.99	1.834	20.050	1.873	20.457
N4578	2284	−2	0.092	1.127	0.015	19.66	0.22	1.12	1.706	20.894	1.840	21.357

Table 1. Fundamental Plane Data for SBF Survey Galaxies — *continued*

Galaxy	v_h	T	A_B	$(V-I)_0$	\pm	\overline{N}	\pm	PD	$\log R_e^{(I)}$	$\langle \mu_R \rangle_e^{(I)}$	$\log R_e^{(V)}$	$\langle \mu_R \rangle_e^{(V)}$	$\log \sigma$	\pm	Mg ₂	\pm
N4594	1128	1	0.221	1.175	0.031	1.04	1.994	19.044	2.361	0.022	0.310	0.009
N4600	787	-2	0.116	1.141	0.017	16.08	0.28	1.66	1.210	20.075	1.205	20.032
N4616	4585	-4	0.549	1.196	0.021	20.31	0.29	2.36	1.408	20.701	1.184	20.111	2.243	0.031	0.267	0.014
N4620	1178	-2	0.126	1.048	0.019	17.89	0.35	1.51	1.381	20.951	2.091	23.017
N4621	444	-5	0.144	1.172	0.018	21.22	0.27	1.62	1.697	19.520	1.672	19.464	2.336	0.014	0.308	0.004
N4636	937	-5	0.120	1.233	0.012	21.45	0.23	1.29	1.974	20.493	2.185	21.091	2.297	0.009	0.300	0.003
N4638	1148	-3	0.110	1.149	0.013	19.89	0.32	1.23	1.190	18.542	1.246	18.758
N4645	2593	-4	0.639	1.188	0.025	20.66	0.24	2.13	1.364	19.531	1.371	19.557	2.283	0.009	0.278	0.004
N4649	1095	-5	0.115	1.232	0.023	21.83	0.22	0.86	1.619	18.634	1.630	18.702	2.531	0.008	0.329	0.003
N4684	1589	-1	0.119	1.100	0.015	18.35	0.26	2.68	1.259	19.152	1.203	19.030
N4696	2958	-4	0.490	1.203	0.014	22.40	0.25	2.53	1.760	20.212	1.774	20.277	2.398	0.018	0.276	0.007
N4697	1210	-5	0.132	1.157	0.010	20.71	0.23	2.19	1.850	19.749	1.822	19.650	2.215	0.008	0.278	0.004
N4709	4650	-5	0.513	1.199	0.011	21.77	0.30	1.80	1.776	20.860	1.896	21.236	2.388	0.008	0.328	0.003
N4725	1207	2	0.051	1.209	0.023	20.71	0.38	1.82	1.898	20.516	1.933	20.677
N4729	3293	-4	0.543	1.219	0.028	20.34	0.34	3.04	1.454	20.451	1.428	20.367	2.154	0.009	0.276	0.004
N4742	1321	-5	0.176	1.045	0.017	18.47	0.24	1.84	1.164	18.588	1.158	18.421	1.969	0.024	0.158	0.006
N4754	1374	-3	0.143	1.178	0.011	20.27	0.23	1.82	1.539	19.510	1.661	19.921
N4767	3005	-5	0.461	1.175	0.028	20.85	0.29	2.80	1.329	19.289	1.361	19.377	2.319	0.016	0.291	0.005
N4802	1013	-2	0.206	1.004	0.018	17.66	0.24	1.63	1.347	19.477	1.344	19.415
N4826	414	2	0.178	1.029	0.011	19.88	0.27	0.77	1.816	18.803
N4946	3036	-4	0.475	1.190	0.021	21.33	0.24	2.45	1.449	20.295	1.359	19.964	2.309	0.025	0.303	0.010
N5011	3099	-5	0.427	1.189	0.027	21.95	0.27	2.73	1.595	20.112	1.466	19.645	2.390	0.017	0.272	0.006
N5044	2704	-5	0.301	1.210	0.027	21.23	0.32	2.18	1.406	19.367	1.412	19.422	2.365	0.039	0.320	0.007
N5061	2040	-5	0.296	1.099	0.023	21.07	0.30	3.13	1.667	19.666	2.301	0.022	0.241	0.006
N5090	3376	-5	0.621	1.210	0.032	22.64	0.39	2.77	2.027	21.463	2.013	21.360	2.440	0.021	0.315	0.007
N5193	3644	-5	0.243	1.164	0.034	20.54	0.32	2.91	1.371	19.832	1.323	19.677	2.338	0.019	0.300	0.008
N5273	1089	-2	0.043	1.142	0.017	19.14	0.31	1.38	1.593	20.694	2.049	22.049
N5322	1804	-5	0.061	1.183	0.011	22.02	0.30	1.74	1.723	20.042	1.490	19.168	2.342	0.039	0.265	0.007
N5338	777	-2	0.118	1.019	0.023	16.57	0.34	2.05	1.477	21.524	1.496	21.565
N5485	1985	-2	0.072	1.180	0.017	20.35	0.39	2.32	1.440	19.871	1.419	19.825	2.185	0.055	0.283	0.010
N5557	3258	-5	0.025	1.202	0.021	21.30	0.34	3.48	1.488	19.768	1.401	19.455	2.412	0.039	0.305	0.007
N5574	1582	-3	0.135	1.054	0.011	18.34	0.64	2.18	1.036	19.053	1.096	19.235
N5576	1555	-5	0.136	1.098	0.010	20.60	0.23	1.71	1.585	19.909	1.545	19.722	2.264	0.055	0.240	0.010
N5582	1314	-5	0.059	1.145	0.013	20.12	0.30	1.21	1.526	20.573	1.537	20.635	2.124	0.023	0.274	0.006
N5631	1950	-2	0.087	1.122	0.019	20.27	0.30	2.41	1.372	19.467	1.479	19.865
N5638	1648	-5	0.143	1.169	0.011	20.43	0.30	1.79	1.407	19.605	1.381	19.506	2.192	0.009	0.301	0.004
N5687	2200	-3	0.048	1.174	0.013	20.26	0.54	2.68	1.614	20.965	1.704	21.296
N5770	1464	-2	0.167	1.120	0.017	18.48	0.34	1.97	1.160	19.375
N5812	2066	-5	0.376	1.213	0.015	21.18	0.34	2.35	1.608	20.138	1.596	20.010	2.301	0.009	0.313	0.004
N5813	1963	-5	0.246	1.189	0.014	22.06	0.26	1.20	1.847	20.709	1.980	21.177	2.356	0.009	0.297	0.004
N5831	1683	-5	0.257	1.140	0.010	20.32	0.25	1.14	1.478	20.002	1.505	20.099	2.211	0.009	0.278	0.004
N5839	1211	-2	0.227	1.190	0.011	19.12	0.36	1.24	1.215	19.749	1.432	20.532
N5846	1709	-5	0.238	1.227	0.007	21.90	0.28	1.02	1.742	19.996	1.725	19.930	2.365	0.008	0.313	0.003
N5866	672	-1	0.058	1.121	0.009	20.27	0.22	0.87	1.566	19.156	1.563	19.230
N5869	2110	-2	0.233	1.161	0.014	19.73	1.24	2.24	1.290	19.556	1.321	19.698
N5898	2090	-5	0.629	1.169	0.009	21.05	0.32	2.12	1.466	19.511	1.506	19.659	2.353	0.013	0.302	0.004
N5903	2518	-5	0.638	1.142	0.011	21.37	0.30	2.28	1.629	20.182	1.629	20.174	2.306	0.016	0.287	0.005
N5982	2936	-5	0.078	1.166	0.010	21.77	0.68	2.83	1.537	19.986	1.558	20.067	2.385	0.023	0.285	0.006
N6305	2770	-3	0.441	1.147	0.051	18.92	0.28	2.33	1.206	19.308	1.055	18.764	2.242	0.041	0.249	0.014
N6411	3690	-5	0.249	1.156	0.008	20.13	0.40	3.35	1.467	20.342	1.429	20.238	2.236	0.016	0.269	0.004
N6483	4880	-5	0.257	1.152	0.051	20.62	0.47	3.33	1.272	19.850	1.122	19.285	2.353	0.042	0.277	0.010
N6502	4880	-4	0.267	1.191	0.041	20.84	0.30	3.81	1.398	20.367	1.259	19.851
N6548	2169	-2	0.353	1.244	0.009	20.68	0.28	1.77	1.655	20.686	1.918	21.531
N6684	865	-2	0.291	1.116	0.015	20.05	0.30	1.07	1.719	19.912	2.002	20.814	2.006	0.013	0.222	0.004
N6702	4725	-5	0.473	1.149	0.006	21.07	0.30	2.71	1.401	20.193	1.527	20.634	2.250	0.008	0.254	0.004
N6703	2370	-3	0.383	1.164	0.006	20.85	0.35	2.02	1.590	20.097	1.598	20.123	2.266	0.008	0.267	0.003
N6851	3043	-5	0.202	1.137	0.016	20.49	0.28	2.04	1.253	19.286	1.235	19.223	2.267	0.042	0.279	0.010
N6861	2819	-3	0.234	1.221	0.019	21.04	0.40	2.47	1.359	19.149	1.312	19.005
N6868	2876	-5	0.237	1.230	0.009	21.43	0.31	2.77	1.479	19.304	1.501	19.385	2.464	0.030	0.333	0.007
N6869	2739	-2	0.790	1.164	0.007	20.62	0.29	2.34	1.375	19.658	1.285	19.352
N6876	3951	-5	0.195	1.178	0.009	21.89	0.43	3.36	1.429	19.520	1.467	19.650	2.374	0.030	0.300	0.007
N6909	2753	-4	0.164	1.064	0.020	19.95	0.23	2.00	1.420	20.267	1.231	19.585	2.178	0.042	0.218	0.010
N7029	2818	-5	0.159	1.138	0.032	20.77	0.50	2.27	1.249	19.133	1.270	19.189	2.308	0.030	0.266	0.007
N7041	1877	-3	0.173	1.139	0.055	20.21	0.27	1.66	1.347	19.337

Table 1. Fundamental Plane Data for SBF Survey Galaxies — *continued*

Galaxy	v_h	T	A_B	$(V-I)_0$	\pm	\overline{N}	\pm	PD	$\log R_e^{(I)}$	$\langle\mu_R\rangle_e^{(I)}$	$\log R_e^{(V)}$	$\langle\mu_R\rangle_e^{(V)}$	$\log \sigma$	\pm	Mg ₂	\pm
N7049	2158	-2	0.237	1.174	0.033	21.54	0.25	1.58	1.448	19.002	1.483	19.237
N7097	2404	-5	0.085	1.176	0.022	20.26	0.27	1.55	1.182	19.133	1.191	19.192
N7144	1921	-5	0.091	1.161	0.009	20.63	0.22	1.65	1.592	20.140	1.652	20.361	2.272	0.042	0.291	0.010
N7145	1874	-5	0.091	1.133	0.016	20.12	0.28	1.76	1.583	20.372	1.544	20.236	2.125	0.030	0.258	0.007
N7168	2747	-5	0.101	1.184	0.022	20.50	0.29	2.36	1.336	19.870	1.310	19.756
N7173	2501	-4	0.114	1.150	0.017	19.91	0.26	1.89	1.168	19.211	1.164	19.207	2.293	0.030	0.280	0.007
N7180	1479	-2	0.138	1.109	0.009	17.86	0.32	1.35	1.015	19.083	1.178	19.644	1.987	0.026	0.187	0.006
N7185	1838	-3	0.135	1.080	0.012	18.44	0.41	2.18	1.474	20.884	1.628	21.430
N7192	2879	-4	0.146	1.174	0.032	21.17	0.34	2.60	1.401	19.633	1.414	19.681	2.275	0.042	0.263	0.010
N7196	3007	-5	0.095	1.211	0.022	21.71	0.34	1.86	1.389	19.604	1.414	19.685	2.451	0.042	0.302	0.010
N7200	2897	-4	0.083	1.183	0.018	19.24	0.37	2.03	1.062	19.741	1.026	19.527	2.299	0.042	0.296	0.010
N7280	1903	-1	0.240	1.105	0.009	19.56	0.29	1.67	1.576	20.823	1.950	21.989
N7302	2586	-3	0.299	1.126	0.016	19.19	0.28	2.33	1.201	19.368	1.578	20.692
N7331	819	3	0.392	1.120	0.017	20.75	0.24	0.36	1.702	19.035	1.805	19.521
N7332	1207	-2	0.161	1.107	0.008	19.98	0.28	0.61	1.242	18.648	1.252	18.639
N7454	2007	-5	0.343	1.123	0.012	19.66	0.35	1.23	1.474	20.278	1.325	19.753	2.018	0.009	0.199	0.004
N7457	822	-3	0.228	1.104	0.009	18.99	0.28	0.36	1.626	20.343	1.831	21.015
N7507	1548	-5	0.206	1.196	0.009	21.54	0.25	1.20	1.600	19.494	1.472	19.000	2.369	0.033	0.324	0.007
N7562	3608	-5	0.453	1.187	0.018	21.95	0.85	2.97	1.295	19.278	1.386	19.486	2.394	0.009	0.280	0.004
N7619	3747	-5	0.347	1.229	0.009	22.74	0.37	2.46	1.656	20.330	1.680	20.414	2.510	0.009	0.333	0.003
N7743	1658	-1	0.305	1.080	0.009	19.51	0.25	1.03	1.522	20.145	2.105	22.072
N7796	3252	-4	0.044	1.230	0.022	22.21	0.43	2.43	1.571	20.325	1.608	20.450
N7814	1050	2	0.192	1.245	0.017	20.23	0.22	0.51	1.611	19.734	1.571	19.740
U07767	1331	-5	0.089	1.152	0.019	1.67	1.029	19.611

Table 2. X_{FP} Comparisons

Comparison	Galaxy (type)	N_g	$\langle\Delta X_{\text{FP}}\rangle$ (dex)	rms ^a (dex)	rms(0.30) ^b (dex)
VSBF – ISBF	all	257	+0.002 ± 0.001	0.023	0.019
VSBF – ISBF, no N4111.	all	256	+0.002 ± 0.001	0.021	0.017
VSBF – ISBF	E	122	-0.001 ± 0.001	0.016	0.012
ISBF – SMAC	all	32	-0.030 ± 0.008	0.044	0.030
ISBF – SMAC, no N1553	all	31	-0.033 ± 0.007	0.040	0.028
ISBF – SMAC	E	18	-0.025 ± 0.007	0.029	0.019
VSBF – SMAC	all	32	-0.033 ± 0.008	0.044	0.031
VSBF – SMAC, no N1553	all	31	-0.036 ± 0.007	0.039	0.028
VSBF – SMAC	E	18	-0.028 ± 0.007	0.027	0.018
ISBF – 7S	all	169	-0.036 ± 0.003	0.042	0.031
ISBF – 7S	E	120	-0.033 ± 0.004	0.040	0.029
ISBF – 7S, red ^c	all	134	-0.029 ± 0.003	0.033	0.025
ISBF – 7S, red ^c	E	100	-0.026 ± 0.003	0.028	0.020
VSBF – 7S	all	165	-0.036 ± 0.003	0.039	0.030
VSBF – 7S	E	118	-0.031 ± 0.003	0.036	0.027
VSBF – 7S, red ^c	all	132	-0.030 ± 0.003	0.031	0.025
VSBF – 7S, red ^c	E	99	-0.027 ± 0.003	0.027	0.020
7S – SMAC ^d	all	46	-0.003 ± 0.005	0.036	0.030
7S – SMAC ^d	E	25	-0.013 ± 0.007	0.035	0.031

^a Dispersion for comparisons of $X_{\text{FP}} \equiv \log R_e - 0.33\langle\mu\rangle_e$.^b Dispersion for comparisons of $X'_{\text{FP}} \equiv \log R_e - 0.30\langle\mu\rangle_e$.^c ‘Red’ subsample: restricted to galaxies with $(V-I)_0 \geq 1.135$.^d 7S vs. SMAC comparisons restricted to $cz < 5000$ km s⁻¹ because of problems arising from seeing effects on the 7S data at larger distances.